

NEURAL MECHANISMS IN PROCESSING OF EMOTION IN REAL AND  
VIRTUAL FACES USING FUNCTIONAL-NEAR INFRARED SPECTROSCOPY  
(FNIRS)

by

Dylan Rapanan

A thesis submitted to the  
School of Graduate and Postdoctoral Studies  
in partial fulfillment of the requirements for the degree of

**Masters of Science in Computer Science**

Faculty of Science  
Ontario Tech University  
Oshawa, Ontario, Canada

© Dylan Rapanan 2025

## Abstract

As avatars permeate social media, gaming, and telecommunications, understanding how the brain reads emotions from virtual faces is increasingly important. We recorded functional near-infrared spectroscopy (fNIRS) data from adults viewing real photographs and matched computer-generated faces expressing Anger, Disgust, Fear, Joy, Sadness, Surprise, or Neutral (control). General-linear-model mapping revealed higher activation in virtual faces in the left occipital region, and higher activation in Neutral and Surprise compared to the other emotions in parietal and occipital regions. Functional-connectivity analysis revealed higher connectivity in real faces across the brain, and higher connectivity across the brain in Anger and Fear compared to the other emotions. Collectively, the results demonstrate differences in activation in occipital areas, and differential processing of face and emotion types across the whole brain. These neural signatures provide quantitative targets for refining the realism and emotional efficacy of digital characters in virtual and augmented environments.

## Acknowledgements

\*\* Put your Acknowledgements here. \*\*\*

# Contents

<b>Abstract</b>	ii
<b>Acknowledgment</b>	iii
<b>1 Introduction</b>	<b>1</b>
1.1 Functional Near-Infrared Spectroscopy (fNIRS) . . . . .	2
1.2 Facial Emotion Perception . . . . .	4
1.3 Real vs. Virtual (Avatar) Face Perception . . . . .	6
1.4 Objectives and Hypotheses . . . . .	8
<b>2 Methodology</b>	<b>10</b>
2.1 Participants . . . . .	10
2.2 Stimuli and apparatus . . . . .	12
2.2.1 Stimuli . . . . .	12
2.2.2 Apparatus . . . . .	12
2.3 Design and procedure . . . . .	15
2.3.1 Design . . . . .	15
2.3.2 Procedure . . . . .	15
2.4 Analyses . . . . .	17
2.4.1 fNIRS preprocessing . . . . .	17
2.4.2 Activation magnitude with General Linear Model (GLM) . . . . .	19

Design Matrix . . . . .	19
Contrast Computation . . . . .	20
2.4.3 Network mapping with Functional Connectivity Analysis . . . . .	21
Paired Sample t-tests . . . . .	22
ROI Chord Plots . . . . .	22
Emotion Summary Ratio Plot . . . . .	23
Region Summary Plot . . . . .	23
2.4.4 Memory Task Analysis . . . . .	24
<b>3 Results</b>	<b>25</b>
3.1 Activation magnitude . . . . .	25
3.2 Functional Connectivity Results . . . . .	29
3.3 Memory Task Results . . . . .	35
<b>4 Discussion</b>	<b>37</b>
4.1 Limitations and Future Directions . . . . .	37
4.2 Conclusion . . . . .	37
<b>Bibliography</b>	<b>37</b>
<b>Appendix</b>	<b>45</b>
<b>A GLM Contrasts</b>	<b>46</b>
<b>B Functional Connectivity Contrasts</b>	<b>51</b>
<b>C Memory Task</b>	<b>59</b>
C.1 ANOVA Results . . . . .	59
C.2 Memory Task No Response Distribution . . . . .	60

# List of Tables

A.1	Table of contrast results from the GLM analysis.	46
B.1	Ratio of positive to negative <i>t</i> -values for each contrast. The ratio is calculated as Ratio = (Number of Positive <i>t</i> -values - Number of Negative <i>t</i> -values) / (Number of Positive <i>t</i> -values + Number of Negative <i>t</i> -values). For condition1 > condition2, a positive ratio indicates that condition1 has more positive <i>t</i> -values than condition2, while a negative ratio indicates the opposite.	53
C.1	Two-way ANOVA results for the effect of Face Type and Emotion and their interaction on the correct responses.	59

# List of Figures

2.1	Participant signal quality and inclusion flow . . . . .	11
2.2	Montage and brain region map . . . . .	14
2.3	Experimental paradigm overview . . . . .	16
2.4	Preprocessing steps for fNIRS data . . . . .	17
2.5	Sample design matrix for GLM . . . . .	20
3.1	GLM: Real vs. Virtual Faces . . . . .	25
3.2	GLM: Emotion vs. Neutral . . . . .	26
3.3	GLM: Emotion vs. Surprise . . . . .	27
3.4	GLM: Face Type $\times$ Emotion Contrasts . . . . .	28
3.5	FC: Real vs. Virtual . . . . .	29
3.6	FC: Emotion Contrasts (Fear) . . . . .	30
3.7	FC: Summary of Contrasts by Emotion Pair . . . . .	31
3.8	FC: Count of Significantly Different Channel Pairs by ROI . . . . .	33
3.9	FC: Face Type $\times$ Emotion Contrasts . . . . .	35
3.10	Correct Memory Task Responses by Face Type and Emotion . . . . .	36
B.1	FC: Additional emotion contrasts . . . . .	52
C.1	Memory Task No Response Distribution . . . . .	60

# Chapter 1

## Introduction

Our brains are evolutionarily primed to process faces, as they are crucial for social interactions ([Powell et al., 2018](#)). A central aspect of this facial perception is the interpretation of emotional expressions, which underpins our interactions as social beings. Emotional expressions provide essential information about an individual's internal state and intentions, allowing us to navigate complex social environments. Despite a rich literature examining human emotion perception, it remains unclear how the brain processes these emotional expressions definitively ([Barrett, 2006a](#)). This lack of clarity is particularly relevant as our interactions shift increasingly toward digital platforms featuring virtual representations of human faces.

There has been a dramatic increase in the use of avatars, which are computer-generated representations of humans, across a wide range of platforms, including social media, video games, virtual reality (VR), and augmented reality (AR). As our interactions with avatars become more prevalent, particularly in applications involving communication and social interaction, their ability to convincingly express human-like emotions has become a subject of growing interest ([Kegel et al., 2020](#)). The capacity of avatars to produce recognizable and appropriate facial emotional expressions is key to their social acceptance and utility.

Unlike real human faces, which convey emotion through a complex interplay of subtle muscle movements, virtual faces must rely on pre-programmed or algorithmically generated expressions. These expressions may differ in perceived realism, dynamicity, and authenticity, potentially altering how they are processed by the brain. This raises several important questions: Does processing virtual facial expressions engage the same neural mechanisms as processing real facial expressions? Do different emotional expressions elicit distinct neural responses in the brain? And finally, is processing emotional expressions in virtual faces fundamentally different from processing emotional expressions in real faces? To address these questions, this thesis investigates the neural mechanisms underlying facial emotion perception in both real and virtual faces using functional near-infrared spectroscopy (fNIRS).

## 1.1 Functional Near-Infrared Spectroscopy (fNIRS)

fNIRS is a non-invasive neuroimaging technique that measures brain activity by detecting changes in Blood Oxygenation Level Dependent (BOLD) signals, which are associated with neural activity, similar to functional magnetic resonance imaging (fMRI). fNIRS works by shining near-infrared light (760-850nm) through the scalp and measuring the amount of light that is absorbed by oxygenated ( $\text{HbO}$ ) and deoxygenated hemoglobin ( $\text{HbR}$ ) in the brain. This is possible through the Modified Beer-Lambert Law, which relates the concentration of hemoglobin to the absorption of light (Kocsis et al., 2006). It is substantially more portable and cost-effective than MRI, tolerates moderate participant movement, and can be deployed in more ecologically valid or naturalistic settings (Yücel et al., 2017). Temporal resolution is moderate, on the order of seconds, which, although inferior to EEG's millisecond fidelity, remains sufficient to capture the hemodynamic responses associated with emotional and cognitive processes. Despite these advantages, fNIRS remains limited to superficial cortical regions; it lacks sensitivity to

deeper subcortical structures such as the amygdala or insula, which play key roles in emotion processing (Sato et al., 2004). Its spatial resolution is also lower than fMRI's, and signal quality can be influenced by factors like hair density and skin pigmentation (Holmes et al., 2024). Beyond systemic noise, fNIRS signals can also be affected by light in the recording environment and interference from participant hair; these issues can be minimized through careful preparation and room setup. These limitations are mitigated through methodological refinements, such as high-density optode arrangements, short-separation channels (Scholkmann et al., 2014), and motion correction techniques (Fishburn et al., 2019; Bergmann et al., 2023).

Analysis methods such as the General Linear Model (GLM), and functional connectivity metrics allows for the identification of distributed activation/connectivity patterns within the cortical regions accessible to fNIRS. In standard fNIRS analyses, brain activation is often assessed using a general linear model (GLM), where the experimental design (modeled as a boxcar or impulse function) is convolved with a canonical hemodynamic response function (HRF) to estimate stimulus-evoked responses in cortical regions (Tak and Ye, 2014). Since fNIRS data tends to be noisy, correlated with physiological signals, is not independent across channels, and is non-uniformly distributed, the GLM is suited for analyzing fNIRS data due to its ability to deal with this noise (Huppert, 2016). The GLM can then be used to estimate the activation of specific brain channels/regions in response to different stimuli, and to contrast these activations across conditions, such as real versus virtual faces or different emotional expressions. While the GLM measures activation in specific channels, functional connectivity analysis examines the temporal correlations between different brain regions, providing insights into how these regions interact during emotional processing. Functional connectivity can be assessed using various methods, including coherence, phase-slope index, and Granger causality (Bastos and Schoffelen, 2016). The most common method for fNIRS functional connectivity analysis is the Wavelet transform coherence (WTC), having been employed in 90

fNIRS studies (Hakim et al., 2023). WTC is calculated by convolving the signals with a wavelet function, such as the Morlet wavelet. WTC measures the strength of shared frequency components between signals in the time-frequency domain, allowing for the assessment of how connectivity patterns change over time, a key advantage when analyzing non-stationary physiological signals from fNIRS. Additionally, WTC can detect both in-phase and out-of-phase relationships between channels, which is particularly valuable for distinguishing neural signals from physiological noise from fNIRS recordings.

Critically, fNIRS demonstrates strong sensitivity to the prefrontal cortex (PFC), a region heavily implicated in the perception, interpretation, and regulation of emotion (Westgarth et al., 2021; Bendall et al., 2016). Although prior studies have examined facial emotion perception and avatar realism independently, few have explored their interaction within the same neuroimaging paradigm. Even fewer studies have employed fNIRS to do so. To our knowledge, no existing research has directly compared neural responses to emotional expressions in real versus virtual faces using a within-subject fNIRS design. This gap limits our understanding of how face realism and emotion interact to shape cortical activation patterns and functional connectivity during social perception. Addressing this gap will provide insights into how digital representations of human emotion are processed and perceived in the brain.

## 1.2 Facial Emotion Perception

There are three main core areas of emotion processing: emotion perception, experience, and regulation (Westgarth et al., 2021). Emotion perception involves recognizing social cues such as facial emotional expressions, which is the focus of this thesis. Human facial emotion perception has been a central topic in affective neuroscience, with Ekman and Friesen (1971) identifying a set of basic emotions that are universally recognized across cultures. Ekman proposed six basic emotions: happiness, sadness, anger, fear,

disgust, and surprise. As well, neutral faces serve as a baseline in many experiments, in addition to these basic emotions. These emotions are reliably associated with distinct facial configurations, known as the Facial Action Coding System (FACS), developed by [Ekman and Friesen \(1978\)](#), which provides a comprehensive taxonomy of facial muscle movements, known as action units, which underpin the visible expressions of emotion. FACS categorizes facial movements into action units (AUs), each corresponding to specific muscle contractions, such as the raising of the eyebrows or the curling of the lips. This system has informed both psychological research and the development of synthetic facial expression systems in virtual environments.

Datasets are crucial for studying facial emotion perception, as they provide standardized stimuli for experimental manipulation and analysis. The UIBVFED dataset is an example of a dataset that utilizes blendshapes to represent facial expressions in virtual characters ([Oliver and Amengual Alcover, 2020](#)). The UIBVFED dataset contains a set of 20 virtual characters that are also ethnically diverse, aged 20-80 years old expressing 32 emotions. The UIBVFED facial expressions were created using blendshapes, a tool that represents and manipulates clusters of facial landmarks similar to that of facial action units (AUs). The racially diverse affective expression (RADIATE) face stimulus set is another dataset that enables the study of facial emotion perception using real human faces ([Conley et al., 2018](#)). The RADIATE contains perceptually validated images of racially and ethnically diverse participants, aged 18-30 years old, each expressing 16 different emotions. The validity ratings indicated that the images were accurately perceived as expressing the intended emotions. These datasets provide a rich resource for examining how different facial expressions, whether from real or virtual faces, are processed in the brain.

More recent approaches, however, advocate a constructionist view of emotion. According to [Barrett \(2006b\)](#), emotions are not fixed categories but constructed experiences emerging from the brain's interpretation of internal and external stimuli. [Lindquist et al.](#)

(2012) argue that emotions arise from distributed and context-sensitive neural activity involving domain-general brain networks rather than discrete, emotion-specific regions. This debate has significant implications for avatar perception, if emotions are constructed rather than discrete, then the realism, dynamicity, and context of avatar expressions may critically shape how they are interpreted and processed neurologically. There is increasing evidence supporting this involvement of domain-general networks in emotion perception.

While multivariate pattern analysis (MVPA) studies have shown that both localized and distributed neural patterns can predict emotional states (Kragel and LaBar, 2016), findings remain inconsistent, especially in the prefrontal cortex (PFC) (Westgarth et al., 2021; Bendall et al., 2016). Some fNIRS studies report increased PFC activation during facial emotion recognition (e.g., in the ventral and medial PFC), others find decreased or no significant changes in oxygenated hemoglobin (HbO) levels. Even studies using similar facial expression tasks report varying activation patterns depending on the specific emotion or cortical region involved. For instance, happy and fearful faces have been associated with increased right PFC activation, whereas sad faces tend to elicit decreased activation in the left PFC. These mixed findings echo fMRI research, which implicates a wide network, including the medial PFC, amygdala, fusiform gyrus, superior temporal sulcus, and insula in emotion perception, with specific emotions such as anger, disgust, and sadness engaging distinct cortical and subcortical areas. These findings underscore the complexity of emotion processing and highlights the need for more nuanced investigations of how different emotional expressions are represented in the brain.

### 1.3 Real vs. Virtual (Avatar) Face Perception

The increasing use of avatars has raised questions about how their facial expressions compare to real human faces. García et al. (2020) designed avatar facial expressions using the FACS that were validated by human observers, demonstrating the efficacy of using

FACS-based design principles to create reliable virtual human facial expressions. Studies have shown that expressions of happiness, anger, fear, and other basic emotions can be accurately interpreted from both static and dynamic virtual avatars (Faita et al., 2015; Dyck et al., 2008). However, in some cases, avatars may convey emotional expressions more or less effectively than real human faces, i.e. Dyck et al. (2008) found that while disgust was challenging to convey using current avatar technology, virtual expressions of sadness and fear were recognized more accurately than their natural face counterparts. Hortensius et al. (2018) provides guiding principles for designing avatars that can effectively convey emotional expressions, and found people are generally less accurate at recognizing emotions from robotic faces compared to human faces. However, virtual agents can be as effective as humans in conveying emotions, particularly when their facial muscle movements are clearly depicted. This work highlights the potential for avatars to convey facial/emotional expressions effectively, but it also raises questions about how these virtual faces are processed in the brain compared to real human faces.

A growing body of affective and cognitive neuroscience research suggests that virtual faces, while often processed similar to real faces, can still elicit distinct neural responses due to differences in perceived authenticity, dynamicity, and realism. De Borst and De Gelder (2015) note that since humans are highly attuned to perceiving real human faces, viewing avatars may engage different perceptual and neural processes, potentially leading to altered brain activity. As a result, findings from studies using avatars and those using real human faces may not always be directly comparable and should be interpreted cautiously. The mechanisms underlying these differences remain unclear, highlighting the need for further neuroimaging research that systematically compares the physical characteristics of avatars and real faces. For instance, Kegel et al. (2020) demonstrated that fearful human expressions elicited significantly stronger neural responses than fearful avatar expressions in regions including the posterior and anterior superior temporal sulcus, anterior insular cortex, posterior cingulate cortex, and ventral anterior cingulate

cortex, with particularly strong effects observed in both the left and right superior temporal sulcus and inferior frontal gyrus. In contrast, neutral human and avatar expressions did not differ significantly. An EEG study by [Sollfrank et al. \(2021\)](#) used the same dynamic stimuli as [Kegel et al. \(2020\)](#) and found that the avatar faces elicited significantly stronger reactions than the real faces for theta and alpha oscillations. [Park et al. \(2021\)](#) found that observers' responses to avatar facial expressions are modulated by the degree to which the avatar resembles their own appearance and habitual expressions.

These perceptual discrepancies may partially stem from the so-called "uncanny valley" phenomenon ([Mori et al., 2012](#)), wherein highly realistic but imperfect virtual faces evoke a sense of unease or cognitive dissonance in observers. [Kätsyri et al. \(2017\)](#) empirically tested this hypothesis using semirealistic computer-animated film characters and found that characters perceived as more realistic were rated as more 'eerie', compared to the more cartoonish characters. The N170 is an event-related potential (ERP) component, commonly investigated in EEG studies, that is typically observed over occipitotemporal scalp regions and is associated with the early perceptual processing of faces. [Chen et al. \(2024\)](#) found a non-linear modulation of EEG responses to the realness of face images, suggesting that the brain's processing of facial stimuli is sensitive to their perceived authenticity. Similarly, [Schindler et al. \(2017\)](#) tested six face-stylization levels varying from abstract to realistic and found that the N170 was generated more occipitally for abstract/virtual faces than for real faces. These findings suggest that deviations from typical human facial expressions can lead to altered neural processing.

## 1.4 Objectives and Hypotheses

This thesis aims to investigate the neural differences in how humans perceive emotional expressions in real versus virtual faces. We used fNIRS to measure brain activation and functional connectivity while participants viewed both real and virtual faces expressing

various emotions. We hypothesize that 1) there will be significant differences in activation patterns and functional connectivity profiles when comparing virtual faces to real faces, 2) different emotional expressions will elicit distinct activation patterns and functional connectivity profiles. We have no a priori predictions regarding the specific nature of these differences, as they may vary based on the emotional content and the realism of the faces. To date, no study has employed a fully crossed factorial design that systematically examines all basic emotions across both real and virtual face types within a single experiment, particularly using fNIRS. Most prior research has concentrated on a limited subset of emotions (typically fear or anger) and often only with avatars. As a result, our understanding of the interaction between emotion type and face realism remains incomplete across the full range of basic emotions. In doing so, this research contributes to the broader understanding of emotional cognition in the age of digital interaction and informs the design of emotionally expressive avatars for applications in education, mental health, and human-computer interaction.

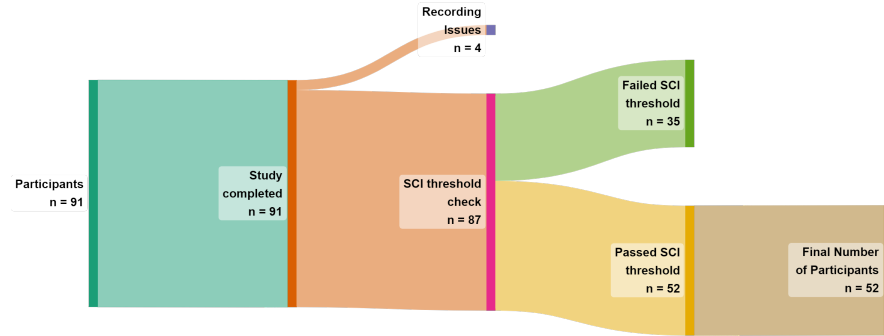
# Chapter 2

## Methodology

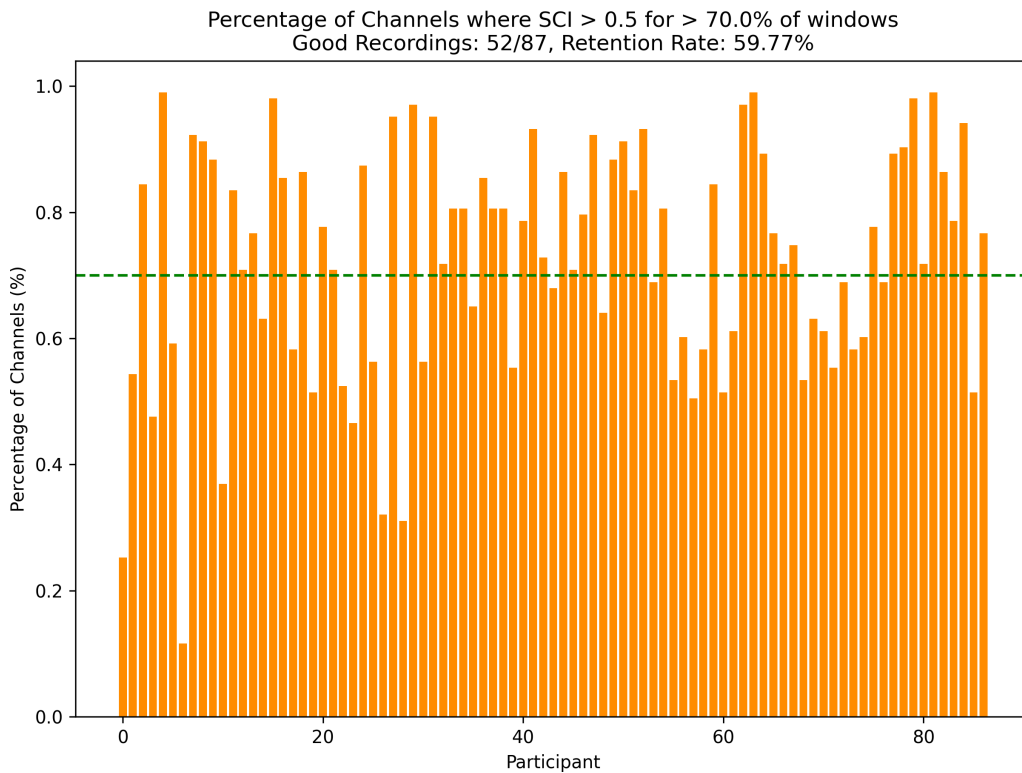
### 2.1 Participants

Ninety-one participants were recruited from Ontario Tech University's undergraduate student body through SONA. Participation flow is illustrated in Figure 2.1a. Four participants were removed due to equipment recording issues. Participants were then screened on inclusion criteria for a) task attention, and b) fNIRS signal quality. For attention, participants were required to achieve  $\geq 60\%$  accuracy on the behavioral memory task (chance accuracy = 50%) to ensure sufficient engagement. One participant failed to meet this criterion. The remaining 87 participants (69 females and 18 males,  $M = 21.09$ ,  $SD = 5.91$ , range = 17 to 51) were analyzed in the behavioral memory task. For neural analyses, signal quality of remaining 87 participants by computing the Peak Spectral Power (PSP) and the Scalp Coupling Index (SCI) (Pollonini et al., 2016). Measures were calculated using a 5-second sliding window across all channels (Bulgarelli et al., 2025; Hernandez and Pollonini, 2020). fNIRS inclusion criteria were: 1) PSP  $> 0.1$  and SCI  $> 0.5$  for more than 70% of the windows in a single channel, labelled "good signal quality" (Holmes et al., 2024), and 2)  $> 70\%$  of the channels for a single participant were marked as "good". Thirty-five participants failed to meet these criteria, illustrated in Figure 2.1b,

and were removed prior to data analysis. The final sample consisted of 52 participants (39 females and 13 males,  $M = 21.62$ ,  $SD = 6.67$ , range = 17 to 51). The study was approved by Ontario Tech's Research Ethics Board (REB: 17656).



(a) Sankey diagram showing the flow of participants through each stage of inclusion/exclusion in the study.



(b) Percentage of Channels where SCI > 0.5 for > 70% of the windows. The green dashed line represents the threshold of 70% of windows that each participant must meet to be included in the analysis.

Figure 2.1: (A) Participant inclusion flow diagram. (B) SCI signal quality inclusion threshold.

## 2.2 Stimuli and apparatus

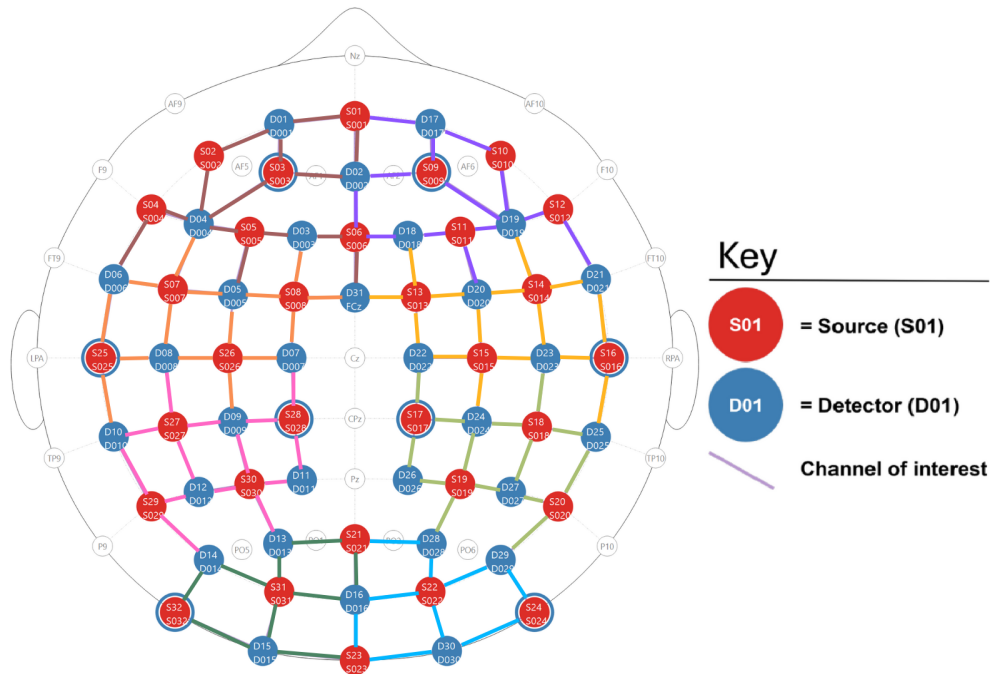
### 2.2.1 Stimuli

One hundred and forty images of facial expressions from the RADIATE and UIBVFED datasets were used ([Conley et al., 2018](#); [Oliver and Amengual Alcover, 2020](#)). Then adult models (5 males and 5 females) from each dataset were identified and matched between-sets on face shape, sex, skin tone, and hair colour. Images of each model expressing seven emotions (anger, disgust, fear, happiness, sadness, surprise, neutral) were selected. Expressions were selected for each model, that closely align with Ekman's 6 basic emotions + neutral ([Ekman and Friesen, 1971](#)). UIBVFED images were cropped to the same size as RADIATE images.

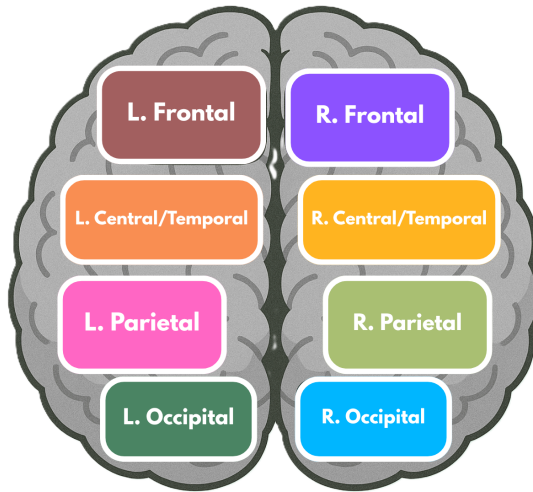
### 2.2.2 Apparatus

Participants were tested individually in a quiet dedicated testing room. Stimuli were presented on a Dell U2415 24-inch monitor at 1920x1200 60Hz. Participants were seated in a comfortable non-movable chair, with the monitor placed at eye level. Stimuli were presented using PsychoPy3 Experiment Builder (v2024.1.5) ([Peirce et al., 2019](#)). Participant brain activity was recorded using Aurora fNIRS while participants completed the task. fNIRS data was collected using two NIRSport2 systems (NIRx Medical Technologies, Berlin, Germany). Each NIRSport2 system was equipped with 16 source and 16 detector optodes, and daisy-chained together for a high density 32x32 optode configuration. Each neighboring pair of source and detector optode is referred to as a channel, resulting in a total of 103 HbO + 103 HbR channels (plus 16 short distance channels). The average distance between source and detector optodes was 30 mm, and 7mm for short distance channels, which were placed on a flexible fNIRS head cap (NIRScap) 58 cm in circumference. The optodes were arranged in a high density 32x32 montage with one bundle of short distance channels, as shown in Figure 2.2. This montage was designed to cover

a maximally large area of the brain, given increasing evidence that emotion processing is not localized to specific discrete areas of the brain, rather distributed across the brain (Lindquist et al., 2012). The fNIRS cap and optodes were positioned following the 10-20 international coordinate system. Light was emitted at 760 nm and 850 nm wavelengths, and the sampling rate was approximately 6.105 Hz.



(a) Depictions of the high density 32x32 optode montage. Red circles represent sources, blue circles represent detectors, the colored lines represent channels, and blue rings around sources represent the locations of the 8 short distance detectors. The colors of the channels represent the regions of interest (ROI's) that the channels were grouped into, see (b) for the corresponding brain region labels.



(b) Brain region map, showing the regions of interest (ROI's) that the channels were grouped into for certain analyses.

Figure 2.2: (a) High density 32x32 optode montage. (b) Brain region map for ROI grouping.

## 2.3 Design and procedure

### 2.3.1 Design

A full-factorial Face-type (2 levels: Real, Virtual)  $\times$  Emotion (7 levels: Anger, Disgust, Fear, Joy, Sadness, Surprise, Neutral)  $\times$  Model (4)  $\times$  Sex (2 levels: Male, Female)  $\times$  Repetition (4) experimental design was used, with each participant presented with 448 images. Stimuli were blocked and counterbalanced by Face-type and Emotion. Within each of the 56 Face-type-Emotion Blocks, participants were presented with 8 distinct model faces (4 male, 4 female).

### 2.3.2 Procedure

Following consent and briefing, participant head size was measured and a size-appropriate fNIRS cap fitted. A signal optimization routine was then run within Aurora fNIRS to optimize participant channel signal levels. This routine worked by increasing source brightness in a stepwise manner, until the optimal signal levels for all channels was reached. Following optimization, participants were told that they would be presented with a series of facial expression images and asked to identify whether a probe face matched one of the faces they saw in the preceding block. Room lights were then switched off to avoid interference with the fNIRS cap, and participants were monitored from an adjacent room with a live camera feed.

The experiment began with instructions presented on screen. The trial timeline, shown in Figure 2.3, consisted of three main epochs: fixation cross, block presentation, and participant feedback. Each Block began with a fixed cross presented for 16 seconds, followed by 8 facial images. Facial images were each presented for 1.5 seconds, with a 250-750 ms ( $M=500$  ms) interstimulus interval (ISI) between each face. To maintain participant attention, participants completed a memory task after each block. In the task, participants were presented with a model image with the same emotional expression as

the rest of the block's images, and asked if the model was shown in the preceding block of 8 faces, with feedback provided using the keyboard (y/n). The probe face has a 50% chance of either being in the previous block or not. The experiment continued after seven seconds if no feedback was provided. Most participants only failed to respond to 1-2 blocks of the 56 blocks, with only a handful of participants failing to respond to up to 5 blocks, as illustrated in Figure C.1. Participants were given a break every seven blocks, and prompted to enter the space bar when they are ready to continue the experiment. After the experiment was completed, the experimenter(s) entered the room, removed the fNIRS cap, and the participant was debriefed about the experiment. Participation in the experiment took approximately 35 minutes.

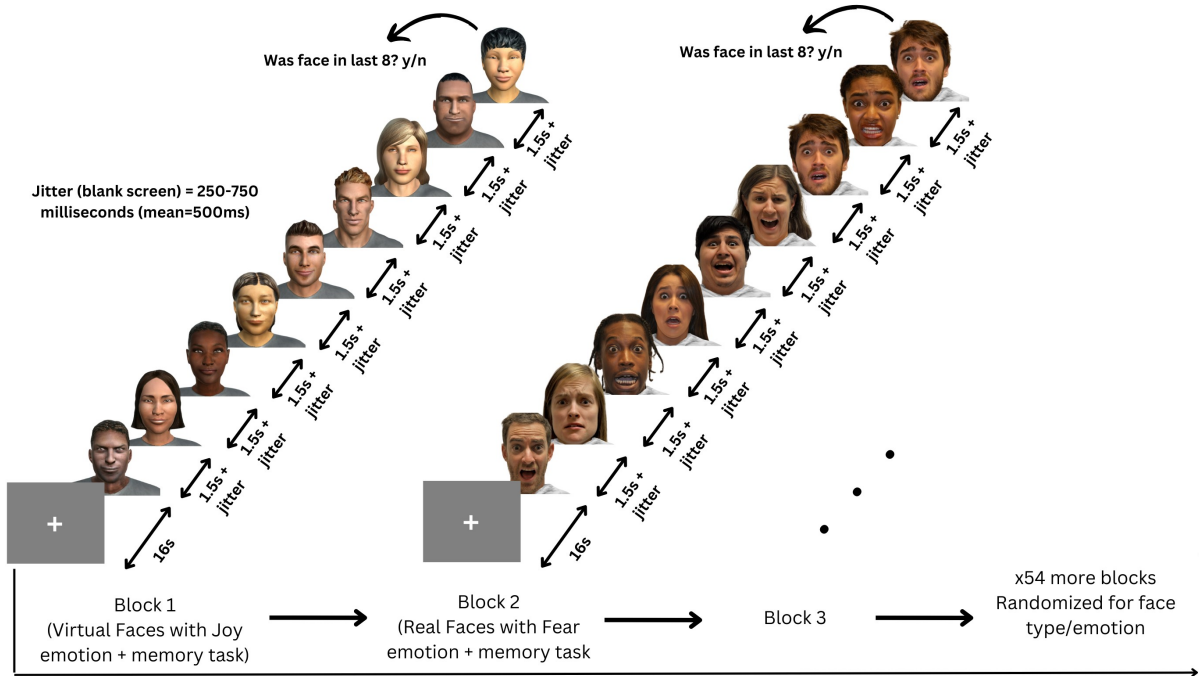


Figure 2.3: Participants viewed 56 blocks of 8 faces, each block being either all real or all virtual faces. Every face in a block displayed the same emotional expression, one of: anger, disgust, fear, happiness, sadness, surprise, neutral.

## 2.4 Analyses

All fNIRS data was preprocessed and analyzed with Python 3.11.9 using MNE (version 1.9.0) (Gramfort et al., 2013) and MNE-NIRS (version 0.7.1) (Luke et al., 2021), which used the Nilearn package (version 0.9.2). Data were analyzed with a General Linear Model (GLM), followed by a functional connectivity analysis. The memory task was analyzed in Python using the statsmodels package (version 0.14.4) (Seabold and Perktold, 2010).

### 2.4.1 fNIRS preprocessing

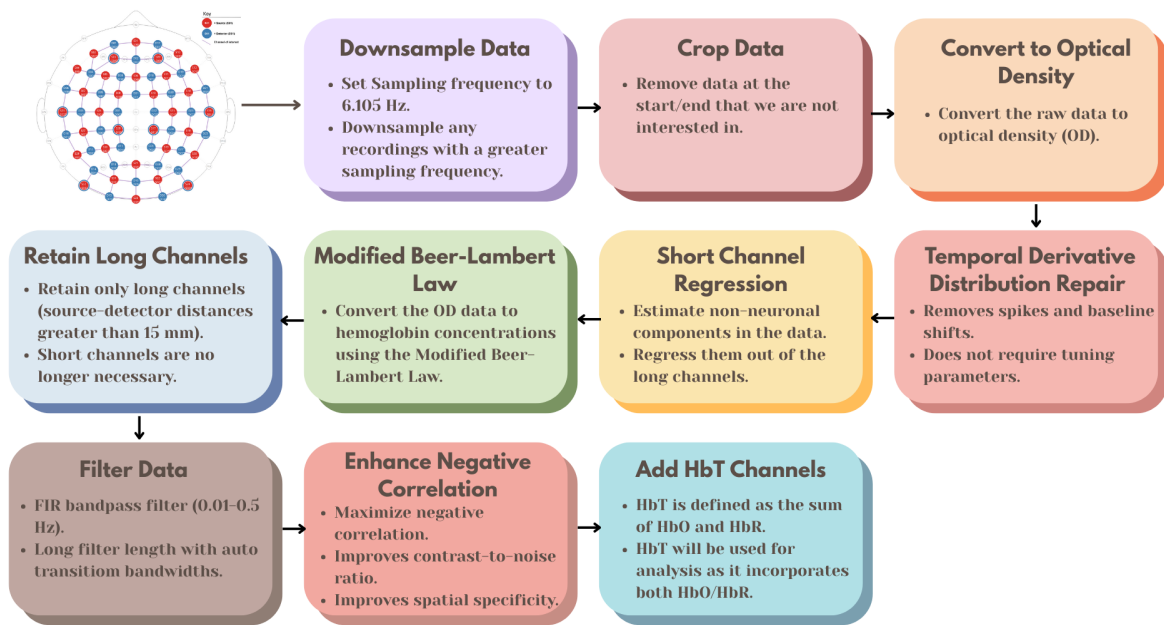


Figure 2.4: Preprocessing steps for fNIRS data, from the raw data to the fully processed data.

The preprocessing steps for the fNIRS data, as shown in Figure 2.4, were as follows:

- 1) Downsample the data if the sampling frequency is greater than 6.105 Hz, the initial two datasets were sampled higher than 6.105 Hz, and the sampling frequency should be consistent across all datasets.
- 2) Crop the data to the first and last annotation. This gets

rid of the extra data at the beginning and end of the recording that are not of interest. 3) Convert the raw data to optical density. 4) Apply temporal derivative distribution repair to the OD data ([Fishburn et al., 2019](#)). TDDR is effective at removing spikes and baseline shifts from the data. 5) Apply short channel regression to the OD data ([Scholkmann et al., 2014](#)). Short channels are used to estimate the superficial hemodynamics (non-evoked/extracerebral/systemic components) in the data, and then regress it out of the long channels ([Tachtsidis and Scholkmann, 2016](#)). 6) Convert the OD data to hemoglobin concentrations using the modified Beer-Lambert law. The MBLL relates the change in light attenuation to the change in hemoglobin concentration of chromophores in the tissue ([Kocsis et al., 2006](#)). 7) Retain only long channels (source-detector distance > 15 mm). Since the short channels have already been regressed out, it is no longer necessary to keep them in the data. 8) This FIR bandpass filter extracts signal components in the 0.01-0.5 Hz range, it uses a long filter length (2015 samples) with automatically determined transition bandwidths by MNE-Python ([Pinti et al., 2019](#)). 9) Maximizes negative correlation between HbO and HbR ([Cui et al., 2010](#)). This method removes spikes, improves contrast-to-noise ratio, and improves spatial specificity of the data. 10) Add HbT (hemoglobin total) channels to the data. HbT is defined as the sum of HbO and HbR. Often, fNIRS studies will only use either one of HbO or HbR channels (more frequently HbO), leaving out one channel with no justification ([Kinder et al., 2022](#)). Therefore, HbT channels are chosen, as HbT makes use of both HbO and HbR channels, and using both hemoglobin species improves the inferences as to where activation occurs [Hocke et al. \(2018\)](#).

Variable length epochs were created for each block of 8 faces, which were 14-18 seconds long (mean = 16s), depending on the ISI's (see [2.3.2](#)). Epochs were sorted by Face Type (Real, Virtual), and Emotion (Anger, Disgust, Fear, Happiness, Sadness, Surprise, Neutral), and their interaction. Baseline correction was applied to remove any constant or slowly varying offsets in the data. The data was annotated with the onsets and offsets

of each block, along with the duration and condition of each block. Block data were then analysed using a GLM and Functional Connectivity analysis.

### 2.4.2 Activation magnitude with General Linear Model (GLM)

The General Linear Model (GLM) posits that the observed haemodynamic signal at each channel or Region of Interest (ROI) is a linear combination of task-related regressors convolved with a Hemodynamic Response Function (HRF), plus nuisance regressors (e.g., drift) and residual noise. Mathematically,

$$Y = X\beta + \epsilon, \quad (2.1)$$

where  $Y$  is the observed time series,  $X$  is the design matrix,  $\beta$  represents the parameters to estimate, and  $\epsilon$  denotes the residuals assumed to be Gaussian noise. Estimation is performed via ordinary least squares (OLS), yielding parameter estimates that quantify condition-specific activation amplitudes.

#### Design Matrix

For each of the epochs, events are defined by their trial type (e.g., emotion or face type), and onsets/offsets relative to the procedure start, and duration. The design matrix is constructed using Nilearn's `make_first_level_design_matrix` by convolving a boxcar function (based on the event timing) with a canonical HRF, which is a model of the expected haemodynamic response to neural activity. The canonical HRF Statistical Parametric Mapping (SPM) (Friston, 2007) is chosen to model neurovascular coupling, this model captures the stereotypical rise and fall of the BOLD/fNIRS response. The cosine drift model was utilized, which incorporates discrete cosine transform (DCT) basis functions into the design matrix to model and remove low-frequency drifts. The selection of the high pass cutoff frequency is guided by the structure of the experimental design.

The cutoff period is set to twice the duration of the longest inter-trial interval, and each fixation period between epochs (or blocks) is 16 seconds. Therefore, a cutoff period of 32 seconds (i.e., `high_pass=0.03125 Hz`) would be appropriate. This ensures that the drift model does not remove task-related signal components that occur at frequencies higher than the cutoff (Luke et al., 2021). The design matrix  $X$  and preprocessed time series are fed into MNE’s `run_glm` function, which computes OLS estimates of  $\beta$  for each channel.

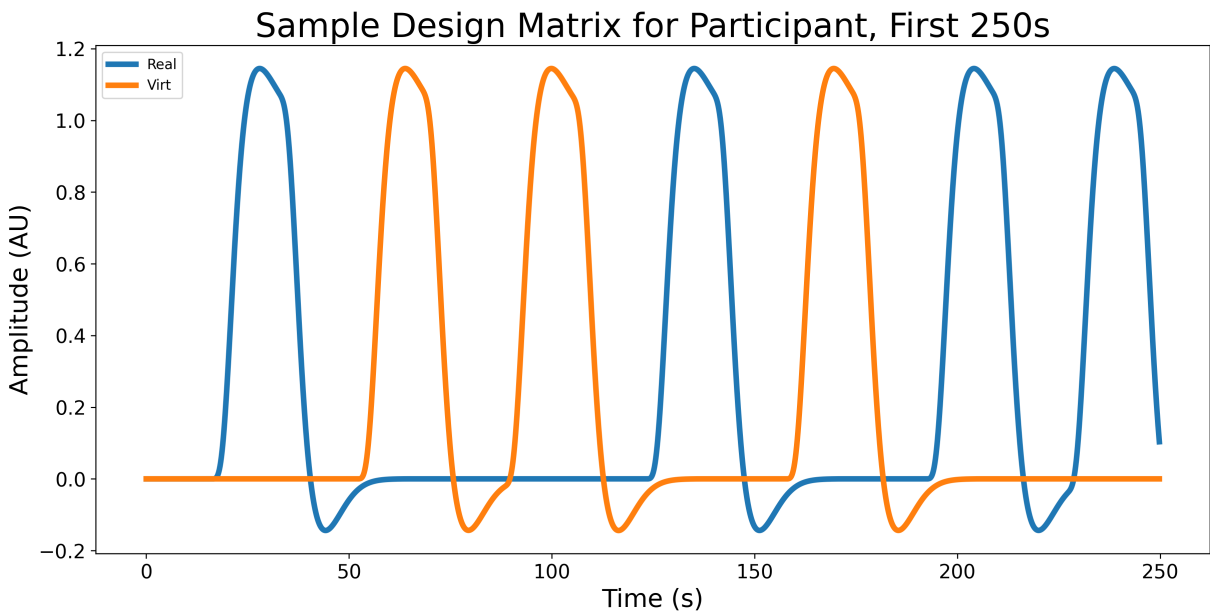


Figure 2.5: Sample design matrix for a single participant for the effect Face type, showing the first 7 blocks (250 seconds) of a single experiment. The design matrix is organized by condition (Blue for real, orange for virtual), this is the result of convolving the boxcar function with the canonical HRF SPM.

A two-way repeated measures GLM was conducted on participant’s HbT responses by Face-type (2 levels: Real, Virtual) and Emotion (7 levels: Anger, Disgust, Fear, Joy, Sadness, Surprise, Neutral). Pairwise contrasts were then computed between conditions to identify effects of interest.

### Contrast Computation

All pairwise contrasts were generated between conditions by constructing an identity contrast matrix over design columns. For each pair of conditions ( $A, B$ ), the contrast vector

is defined as:  $c = e_A - e_B$ , where  $e_A$  and  $e_B$  are the respective design matrix columns for conditions  $A$  and  $B$ . Contrasts are computed using MNE's `compute_contrast` function, which produces effect estimates and test statistics aggregated across channels. Since numerous statistical tests are performed across channels and contrasts,  $p$ -values were FDR-corrected using the Benjamini-Hochberg procedure ([Singh and Dan, 2006](#)) with a family-wise error rate of  $\alpha=0.05$ .

### 2.4.3 Network mapping with Functional Connectivity Analysis

To characterize the temporal coordination between fNIRS channels during face and emotion processing, functional connectivity matrices were computed using a continuous wavelet transform (CWT)-based spectral connectivity approach. CWT decomposes signals into simultaneous time-frequency representations, providing an optimal framework for fNIRS connectivity analysis by accommodating the non-stationary, physiological nature of hemodynamic signals. The morlet wavelet, a gaussian function modulated by a sine wave, was picked as they are suited to capture both slow neural rhythms and faster systemic fluctuations in fNIRS data ([Reddy et al., 2021](#)). Wavelet-based approaches have been widely adopted in the fNIRS literature for connectivity and even artifact correction ([Bergmann et al., 2023; Hakim et al., 2023](#)). Coherence combines both phase and amplitude information into a single, normalized index, 0 (no coupling) to 1 (perfect coupling), and is a richer description of coupling than phase-only or amplitude-only metrics ([Bastos and Schoffelen, 2016](#)).

For each participant, MNE's `spectral_connectivity_time` function was applied to compute time-resolved coherence across pairs of channels, the average of this was taken across epochs to obtain a single channel-by-channel connectivity matrix for each condition. Each participants' connectivity matrix was then averaged across participants to obtain a group-level connectivity matrix for each condition. fNIRS hemodynamics predominantly fluctuate in very low frequencies (0.01-0.5 Hz) ([Reddy et al., 2021](#)). The

frequency range was narrowed to five evenly spaced frequencies between 0.2-0.5 Hz due to short epoch length, this range still targets systemic and neurogenic oscillations while avoiding high-frequency noise ([Xu et al., 2017](#)). Averaging across these closely spaced frequencies reduces data dimensionality, simplifying downstream statistical analyses without sacrificing sensitivity to coupling dynamics.

### Paired Sample t-tests

For each mode (Face type/Emotion), and pair of conditions (e.g., Joy vs. Fear), individual-level connectivity matrices were extracted by averaging across epochs to obtain symmetric channel-by-channel coherence matrices. Because coherence values are bounded between 0 and 1 and exhibit skewed distributions ([Miranda de Sá et al., 2009](#)), Fisher's r-to-z transform (`atanh`) was applied to each matrix element to normalize the data prior to parametric testing. Paired *t*-tests for each unique channel pair ( $i > j$ ) were then conducted across participants using SciPy's `ttest_rel`. This directly tests whether mean connectivity differs between conditions, leveraging the paired design to increase statistical sensitivity ([Hu et al., 2023](#)). Given the large number of channel-pair tests, and similar to the GLM analysis above in [2.4.2](#), *p*-values were FDR-corrected using the Benjamini-Hochberg procedure ([Singh and Dan, 2006](#)) with a family-wise error rate of  $\alpha=0.05$ .

### ROI Chord Plots

To distill high-dimensional channel-by-channel connectivity into interpretable inter-regional summaries, we mapped individual fNIRS channels onto anatomically defined ROI's. This includes left and right frontal, central/temporal, parietal, occipital regions of the brain as shown in Figure [2.2b](#), and the channels were grouped into these regions based on their location in the montage. Since multiple channels may map to the same pair of regions (e.g., several left central/temporal channels connecting to several right occipital channels), we calculated the sum of all significant channel-pair connections for each ROI

pair (separately for positive and negative  $t$ -values). We then subtracted the negative sum from the positive sum, resulting in a single integer representing the net connectivity which was positive if the positive connections outweigh the negative ones, and vice versa. We then took the top 15% percentile of each net connectivity value, and set the rest to zero, to show only the strongest connections between regions. The lines were then plotted using a chord diagram, with the line color indicating the direction of the net connectivity (positive or negative), and the line width indicating the magnitude of the net connectivity (the absolute value of the net connectivity).

### Emotion Summary Ratio Plot

To summarize the net connectivity between regions for each emotion, we calculated a ratio of positive to negative connections for each emotion pair. The ratio was calculated by taking the difference of the count of significant channels where the  $t$ -value was positive and the count of significant channels where the  $t$ -value was negative, and dividing it by the total number of significant channels for that emotion pair. This ratio provides a measure of the net connectivity across all ROI's for each emotion, with a positive ratio indicating that one emotion has a stronger net connectivity than the other, and a negative ratio indicating that the other emotion has a stronger net connectivity.

### Region Summary Plot

To summarize the net connectivity across all emotions for each region, we summed the number of significantly different channel pairs between each region pair across all emotions, disregarding the direction of the  $t$ -value. This provides a measure of the net connectivity across all emotions for each region, showing which regions are more connected across all emotions. The 3 regions with the highest and lowest number of significant channel pairs are marked, to emphasize the most/least connected regions across all emotions.

#### 2.4.4 Memory Task Analysis

Raw behavioral data captured from PsychoPy were preprocessed to identify participant keyboard responses. The total correct trials per participant were summed. Since each block of faces was either all real or all virtual, and all had the same emotional expression (as discussed in 2.3.2), each y/n response was labeled with Face type and Emotion. An OLS model was fit with accuracy (converted to numeric 0/1) as the dependent variable and categorical predictors for Face Type, Emotion, and their interaction. The goal is to determine the main effects of these two factors individually, as well as their interaction, on response accuracy. A two-way Type III ANOVA (via `sm.stats.anova_lm(model, typ=3)`) provided  $F$ -statistics and  $p$ -values for main effects and interaction. This version of the ANOVA is especially suitable when interactions are included in the model, as it calculates each effect after accounting for all other terms.

# Chapter 3

## Results

### 3.1 Activation magnitude

#### Neural Responses to real and virtual faces

A main effect of Face type was reported, with pairwise contrasts revealing greater activation for virtual faces compared to real faces, as shown in Figure 3.1.

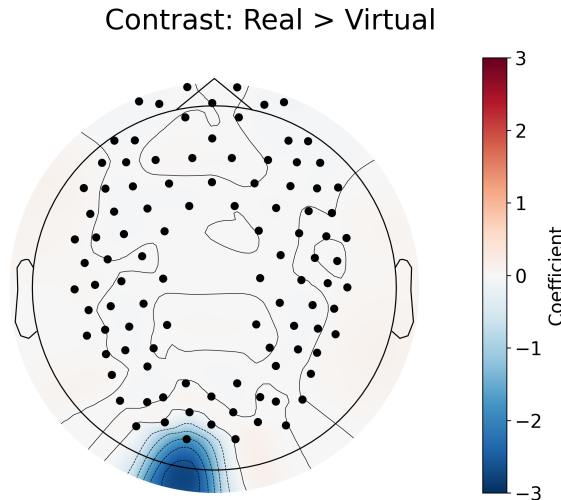


Figure 3.1: GLM contrast between real and virtual conditions which shows the differences in activation between the two conditions. Red signifies that condition 1 (real faces) has more activation in that area than condition 2 (virtual faces), while blue signifies that condition 2 (virtual faces) has more activation than condition 1 (real faces). The color bar on the right shows the coefficient of the contrast, which indicates the strength of the difference in activation between the two conditions.

## Neural Responses to different emotions

Pairwise contrasts with Neutral (control) and other emotions revealed significant differences in activation across several brain regions (Figure 3.2). For instance, perceiving Anger, Fear, and Joy elicited less activity in the right occipital region than perceiving Neutral. Moreover, processing Joy was associated with less activity in the right parietal region, while processing Sadness produced less activity in the left frontal region relative to processing Neutral. These results indicate distinct neural activation patterns for each emotion when contrasted against the "baseline" Neutral condition, with most prominent differences in neural activity over the occipital region.

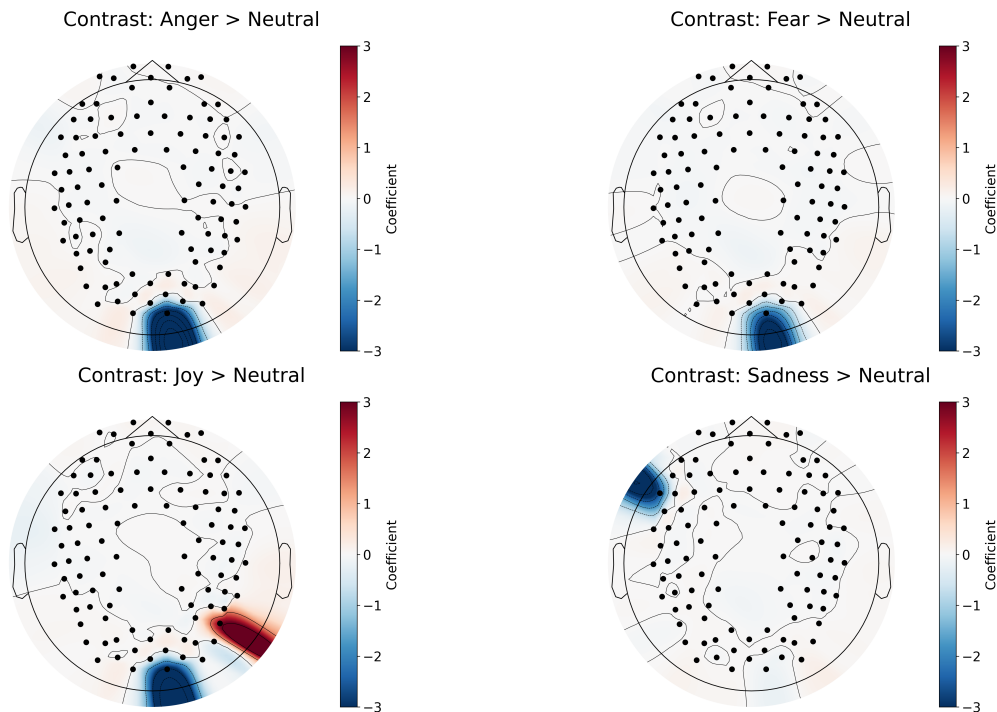


Figure 3.2: GLM results for the contrast between different emotions and neutral condition.

Interestingly, processing Surprise was most consistently different from processing other emotions (Figure 3.3). We found processing Surprise produced 1) more activity in the left central/temporal and right occipital regions relative to processing Disgust and Joy, 2) more activity in the right parietal region relative to processing Fear, 3)

more activity in the left frontal and right parietal regions relative to processing Sadness, and 4) more activity in the right parietal region and less activity in the right occipital region relative to processing Neutral. These findings suggest that Surprise is distinct from processing Neutral but also other emotions, with differences in neural activity more widespread that include central/temporal and parietal regions. All combinations of emotion contrasts were performed, significant differences were only found between Neutral relative to the other emotions, and between Surprise relative to the other emotions.

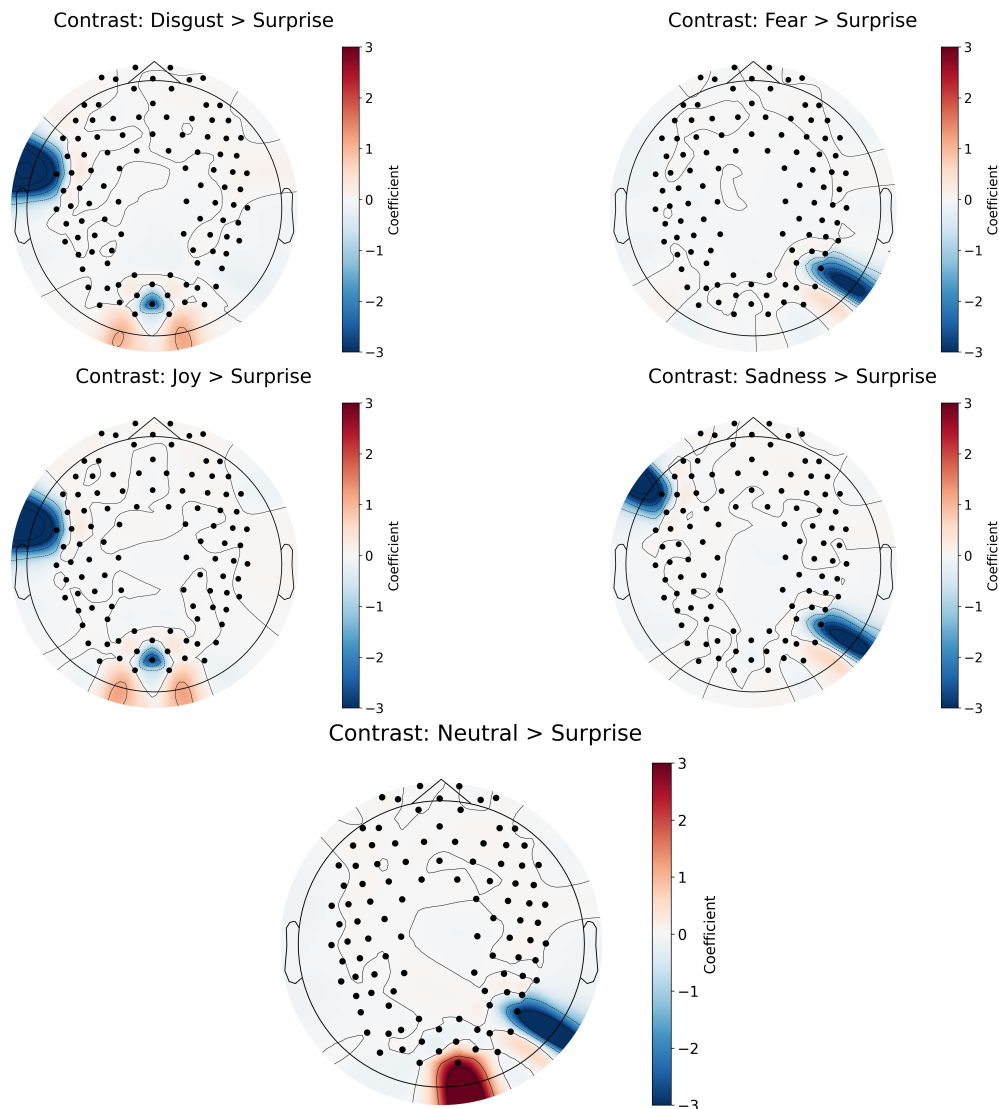


Figure 3.3: GLM results for the contrast between different emotions and surprise condition.

### Differential neural responses to emotions and face type

The interaction of Real > Virtual within each emotion, as shown in Figure 3.4 revealed significant differences in occipital regions exclusively. Specifically, processing Disgust on real faces elicited greater activity in the right occipital region compared to processing Disgust on virtual faces, whereas the left occipital region showed the opposite pattern. Moreover, processing Joy and Neutral emotions on real faces also elicited greater activity in the occipital regions compared to processing the same emotions on virtual faces. We found processing Sadness on virtual faces produced more activity in the left occipital region for virtual faces compared to processing Sadness on real faces. These findings suggest that the neural response to emotional expressions is modulated by the realism of the face stimuli. The full table of the GLM contrasts for all main effects and interactions can be found in Appendix A.

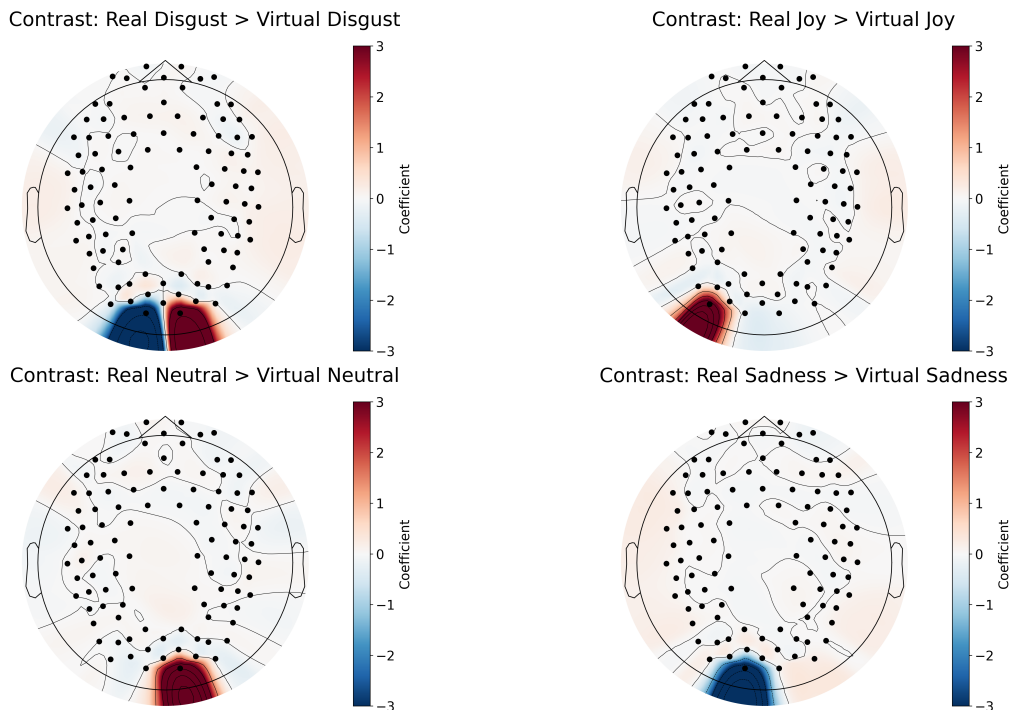


Figure 3.4: GLM results for the contrast between real and virtual conditions within each emotion.

## 3.2 Functional Connectivity Results

### Functional connectivity profiles of face type

The contrast comparing functional connectivity profiles in response to real versus virtual faces (as shown in Figure 3.5) revealed significant differences in connectivity across the brain. Processing real faces was associated with stronger connectivity predominantly between the left to right parietal, left frontal to left parietal, left central/temporal to left parietal, left central/temporal to right parietal, and the right central/temporal to left parietal regions, whereas processing virtual faces was associated with stronger connectivity only between the left central/temporal to right frontal region.

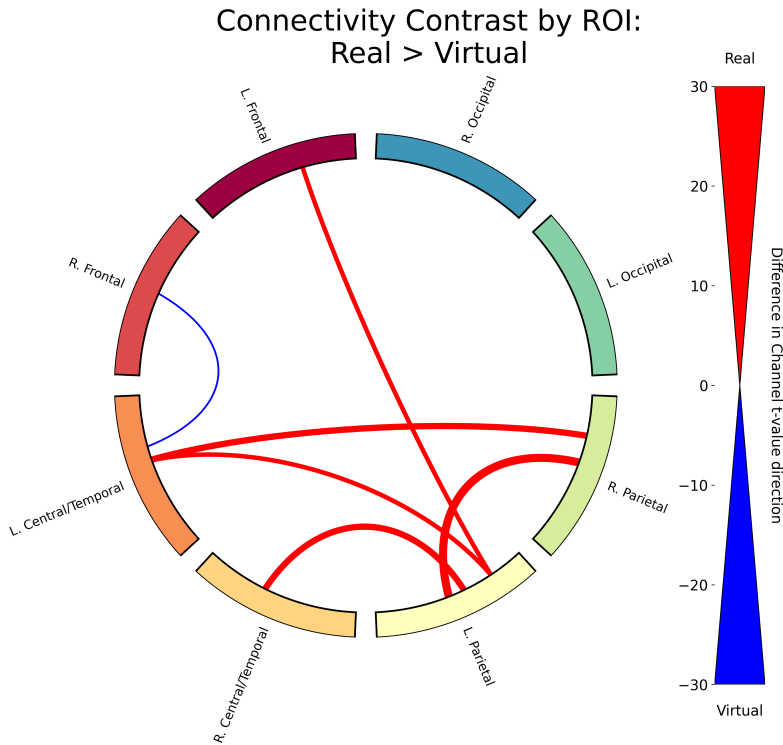


Figure 3.5: Functional connectivity results for the contrast between real and virtual conditions. The thickness of the lines represents the difference in the count of significantly different channel pairs between the two conditions. A red line signifies that real faces had more significant channels between those two ROI's where the  $t$ -value was positive, while a blue line signifies that virtual faces had more significant channels between those two ROI's where the  $t$ -value was negative. For clarity, only the top 15th percentile of connections (those with the most significant different channel pairs) are displayed for all functional connectivity contrasts.

## Functional connectivity in response to emotion

We also found significant differences in functional connectivity in response to different emotions across all ROI's. A sample of the functional connectivity results which include only contrasts between Fear and the other emotions are plotted in Figure 3.6. We found the largest connectivity differences processing faces expressing Fear relative to Neutral faces, with significantly stronger connectivity between left central/temporal and right and left frontal, and right and left parietal. In general, we found processing faces expressing Fear produced significantly strong connectivity across the brain relative to faces expressing all other emotions, however this difference was weakest relative to processing angry faces. Interestingly most of the stronger connections emerge from the left central/temporal region, pointing to this region as a key area for processing Fear. The complete set of functional connectivity contrasts for all emotions can be found in Appendix B.

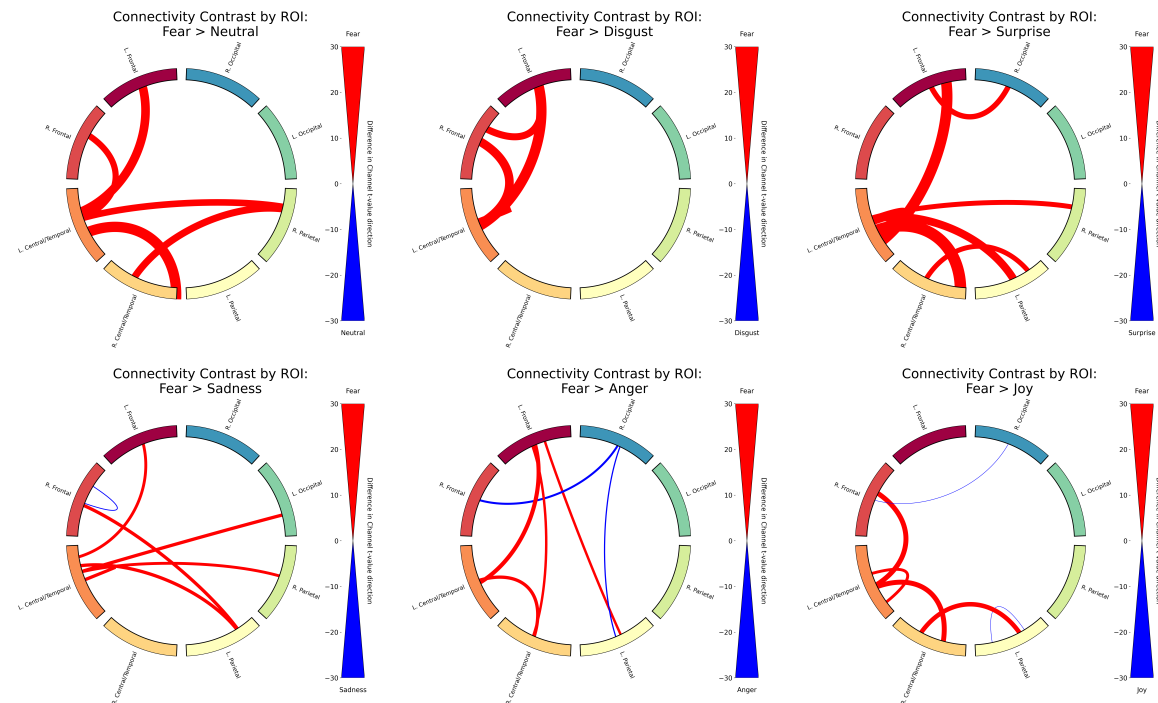


Figure 3.6: Functional connectivity results for Fear relative to the other emotions.

A higher level summary of the functional connectivity results for all emotions is shown

in Figure 3.7, which shows the ratio of significant channels where the  $t$ -value was positive (red) or negative (blue) for each emotion pair. We found a cluster of emotions (Anger, Fear, and Joy) that had much stronger connectivity compared to the other emotions, with Anger and Fear having slightly higher connectivity than Joy. The other emotions (Neutral, Sadness, Surprise) had lower connectivity compared to Anger, Fear, and Joy, with Disgust having higher connectivity than Neutral. This lines up with Figure 3.6, which shows that processing Anger and Fear have higher connectivity relative to the other emotions.

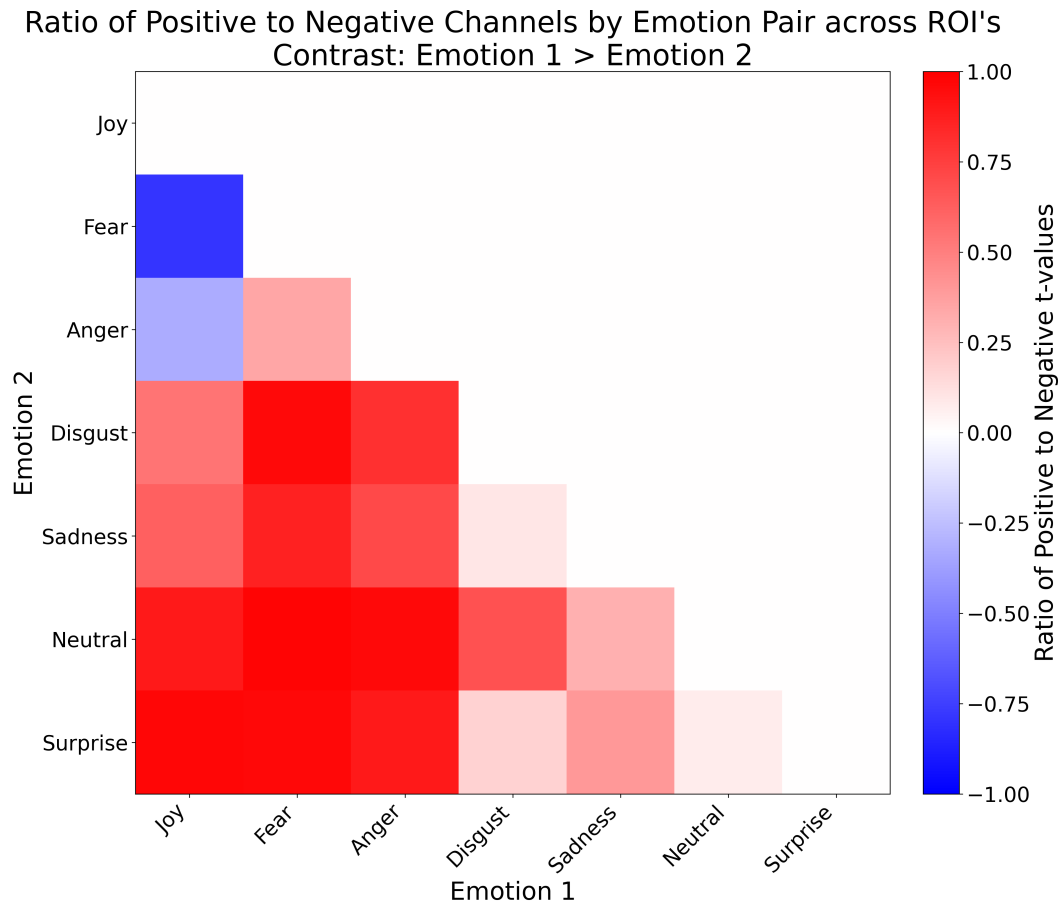


Figure 3.7: A heatmap summary of the functional connectivity results for the contrasts between different emotions across ROI's. Red signifies that emotion 1 had a higher ratio of significant channels where the  $t$ -value was positive, while blue signifies that emotion 2 had a higher ratio of significant channels where the  $t$ -value was negative. The ratio was calculated by taking the difference of the count of significant channels where the  $t$ -value was positive and the count of significant channels where the  $t$ -value was negative, and dividing it by the total number of significant channels for that emotion pair.

To quantify the degree to which ROI's differed across emotion, significant channels across the brain were summed and plotted as a heatmap (Figure 3.8). Two regions, left occipital and right occipital, (marked with an asterisk), produced the least number of significant connections, suggesting that the connectivity within and between these regions are very similar in response to all emotions and that neural indices that differentiate emotion processing likely occur in brain regions outside of visual cortex. Three regions, left central/temporal, left parietal, and right central/temporal (marked with a caret), produced the most number of significant connections, suggesting that these regions are more variable in their connectivity patterns across emotions.

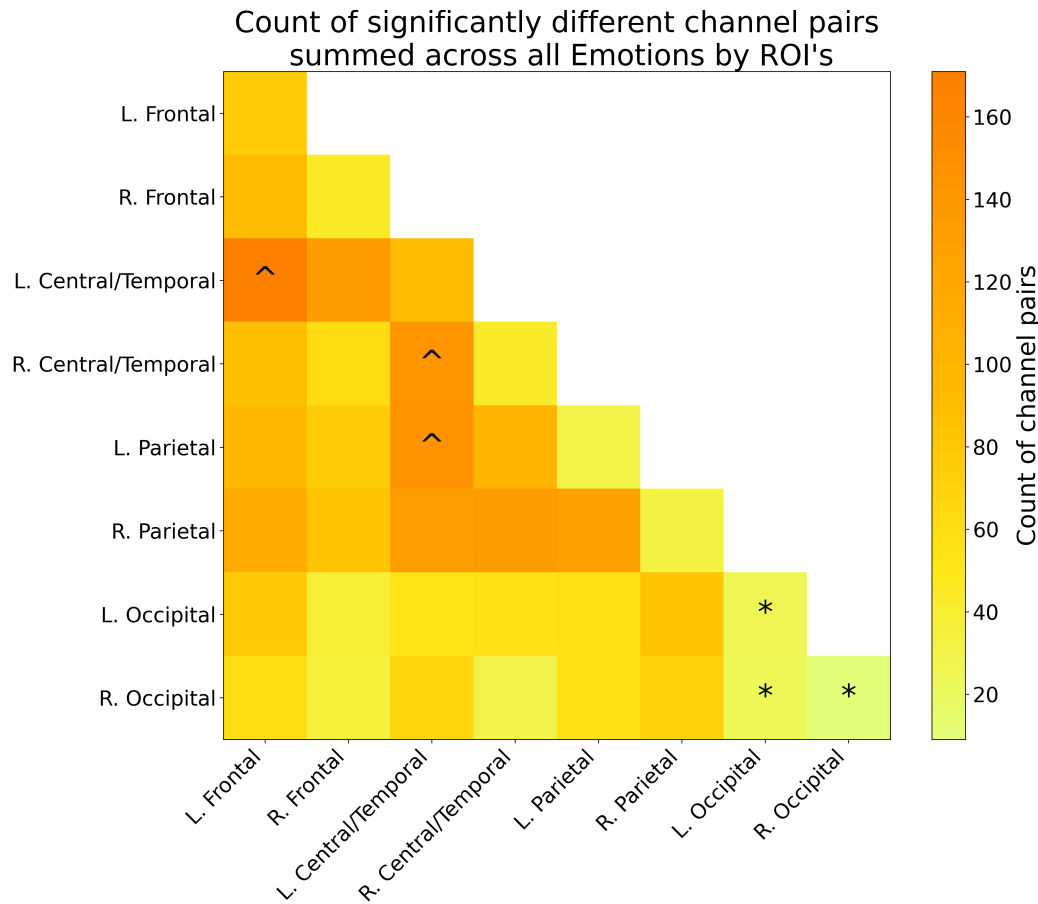


Figure 3.8: A heatmap summary of the number of significantly different channel pairs for each ROI summed across all emotions. The color bar on the right shows the number of significant channel pairs for each ROI, with brighter colors indicating a smaller number of significant channel pairs, and darker colors indicating a larger number of significant channel pairs. An asterisk (\*) was placed on the 3 ROI's with the least number of significantly different channel pairs to indicate that these ROI's are more synchronized with each other than any other pair of ROI's, regardless of the emotion. A caret (^) was placed on the 3 ROI's with the most number of significantly different channel pairs to indicate that these ROI's are less synchronized with each other than any other pair of ROI's, regardless of the emotion. Note that ROI's can have differences within them, as each ROI is made up of multiple channels, and the differences are calculated between channels within the same ROI.

### Differential Functional connectivity profiles in response to emotion across face type

The interaction of face type with emotion, Real > Virtual within each emotion (Figure 3.9) revealed significant differences in functional connectivity across the brain. We

found that processing Anger on virtual faces elicited greater connectivity between the left frontal to right central/temporal, left frontal to right frontal, and within the left frontal region, compared to processing Anger on real faces. Processing Disgust on virtual faces elicited greater connectivity between the left frontal to left parietal, right frontal to left parietal, right frontal to left central/temporal, left frontal to left occipital, and right central/temporal to right parietal, compared to processing Disgust on real faces. Processing Fear on virtual faces elicited greater connectivity between many ROI's, particularly the left frontal to left occipital regions, between the left/right occipital regions, and between the left/right central/temporal and left/right occipital regions, compared to processing Fear on real faces. Processing Neutral on virtual faces elicited greater connectivity between the left frontal to right frontal, left/right frontal to right parietal, and left/right parietal regions, compared to processing Neutral on real faces. Processing Sadness on real faces elicited greater connectivity between the left frontal to right central/temporal, left central/temporal to right parietal, left central/temporal to right occipital, and right central/temporal to left parietal regions, compared to processing Sadness on virtual faces. Processing Surprise on real faces elicited greater connectivity between many ROI's, such as the left frontal to left/right central/temporal, left frontal to right parietal, left-/right central/temporal to left/right parietal, and within the left/right central/temporal regions, compared to processing Surprise on virtual faces. Processing Joy on real faces elicited greater connectivity between the left/right central/temporal to right parietal, and within right parietal regions, whereas processing Joy on virtual faces elicited greater connectivity between the left central/temporal to left/right occipital regions. Overall, these results indicate that the effect of face type on functional connectivity varies by emotion, with virtual faces generally eliciting greater connectivity for negative emotions (Anger, Disgust, Fear, Neutral), while real faces tend to elicit greater connectivity for positive emotions (Sadness, Surprise, Joy), and the specific brain regions involved differ across emotions. Like the GLM results, this indicates that the neural response to emo-

tional expressions is modulated by the realism of the face stimuli. The full table of the functional connectivity contrasts for all main effects and interactions can be found in Appendix B.

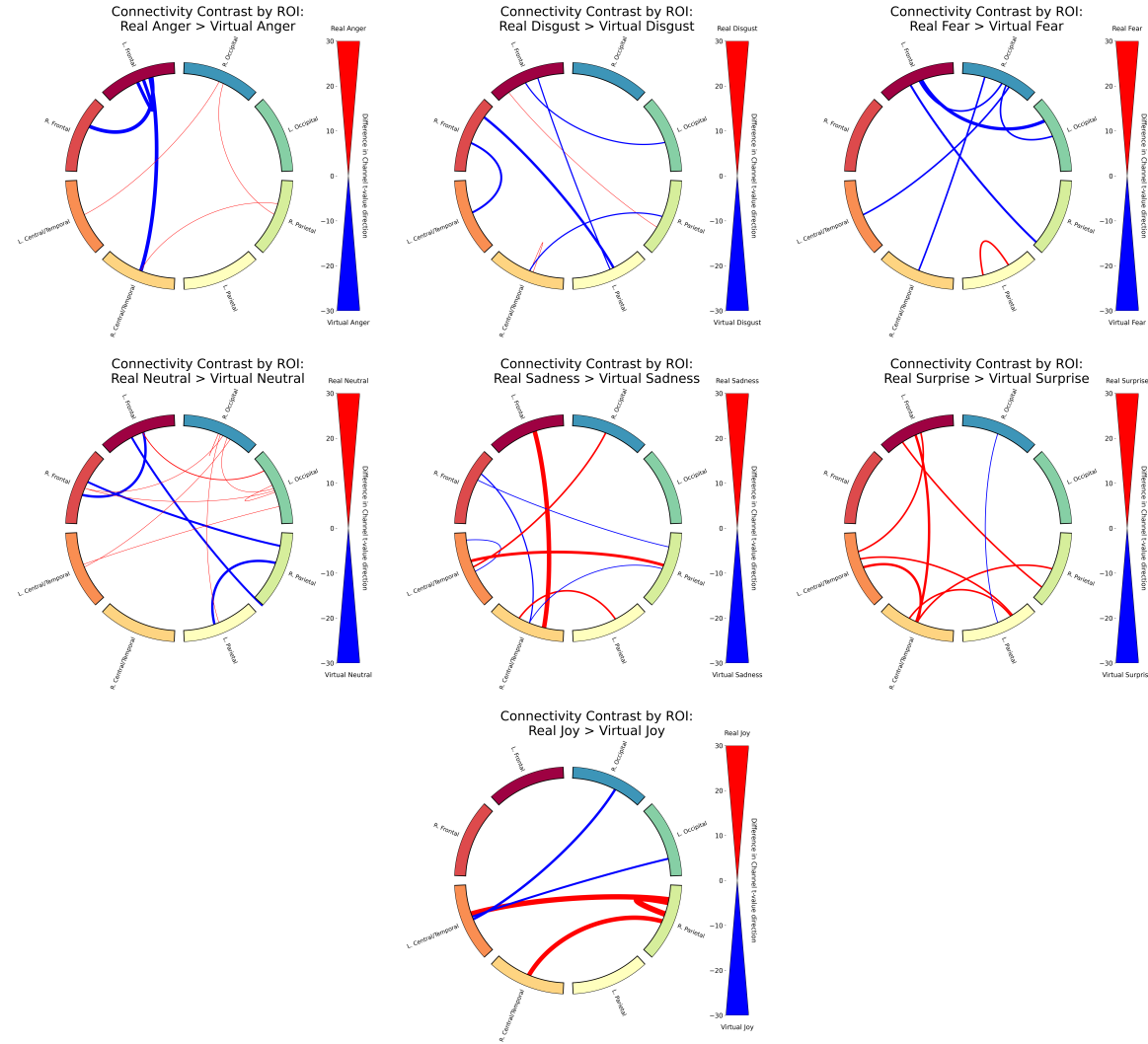


Figure 3.9: Functional connectivity results for the contrast between real and virtual conditions within each emotion.

### 3.3 Memory Task Results

A two-way Type III ANOVA revealed a significant main effect of face type,  $F(1, 4802) = 7.96$ ,  $p = 0.0048$ , indicating that memory performance was higher for real faces com-

pared to virtual faces, as shown in Figure 3.10. There was no significant main effect of emotion,  $F(6, 4802) = 0.83, p = 0.55$ , nor a significant interaction between face type and emotion,  $F(6, 4802) = 0.46, p = 0.84$ . These findings suggest that while the realism of the face influences memory performance, the specific emotional expression does not have a significant impact on memory accuracy. The full ANOVA table is shown in Appendix C.1.

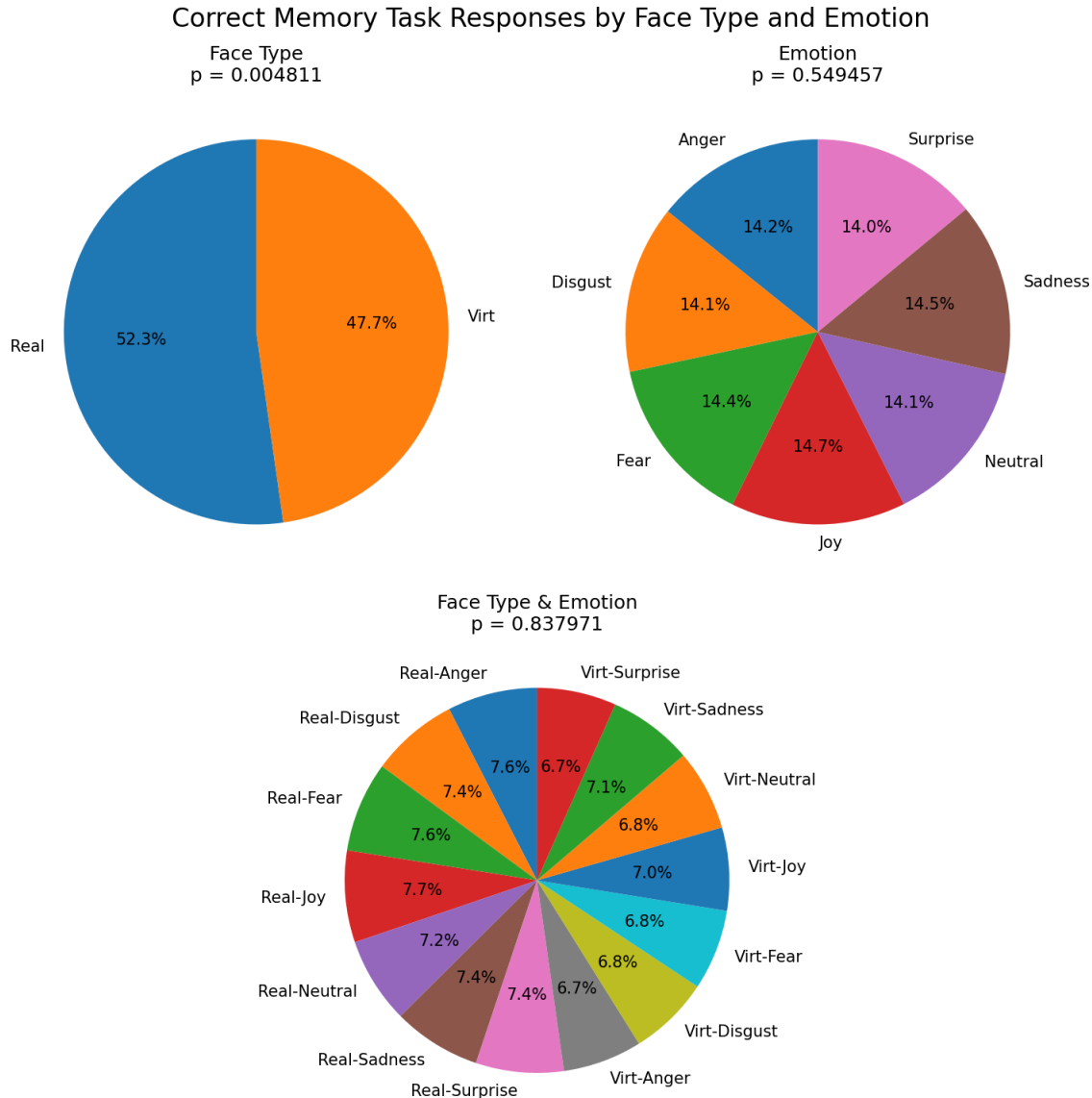


Figure 3.10: Proportion correct by condition in the memory task, plotted separately for real and virtual faces, for each emotion, and the interaction between face type and emotion. The  $p$ -values indicate the significance of the main effects and interaction.

# **Chapter 4**

## **Discussion**

### **4.1 Limitations and Future Directions**

### **4.2 Conclusion**

# Bibliography

- Barrett, L. F. (2006a). Are Emotions Natural Kinds? *Perspectives on Psychological Science*, 1(1):28–58.
- Barrett, L. F. (2006b). Solving the emotion paradox: Categorization and the experience of emotion. *Personality and Social Psychology Review*, 10(1):20–46. PMID: 16430327.
- Bastos, A. M. and Schoffelen, J.-M. (2016). A Tutorial Review of Functional Connectivity Analysis Methods and Their Interpretational Pitfalls. *Frontiers in Systems Neuroscience*, 9. Publisher: Frontiers.
- Bendall, R. C. A., Eachus, P., and Thompson, C. (2016). A Brief Review of Research Using Near-Infrared Spectroscopy to Measure Activation of the Prefrontal Cortex during Emotional Processing: The Importance of Experimental Design. *Frontiers in Human Neuroscience*, 10. Publisher: Frontiers.
- Bergmann, T., Froese, L., Gomez, A., Sainbhi, A. S., Vakitbilir, N., Islam, A., Stein, K., Marquez, I., Amenta, F., Park, K., Ibrahim, Y., and Zeiler, F. A. (2023). Evaluation of Morlet Wavelet Analysis for Artifact Detection in Low-Frequency Commercial Near-Infrared Spectroscopy Systems. *Bioengineering*, 11(1):0.
- Bulgarelli, C., Blasi, A., McCann, S., Milosavljevic, B., Ghillia, G., Mbye, E., Touray, E., Fadera, T., Acolatse, L., Moore, S. E., Lloyd-Fox, S., Elwell, C. E., Eggebrecht, A. T., and Team, t. B. S. (2025). Growth in early infancy drives optimal brain

- functional connectivity which predicts cognitive flexibility in later childhood. Pages: 2024.01.02.573930 Section: New Results.
- Chen, Y., Stephani, T., Bagdasarian, M. T., Hilsmann, A., Eisert, P., Villringer, A., Bosse, S., Gaebler, M., and Nikulin, V. V. (2024). Realness of face images can be decoded from non-linear modulation of EEG responses. *Scientific Reports*, 14(1):5683. Publisher: Nature Publishing Group.
- Conley, M. I., Dellarco, D. V., Rubien-Thomas, E., Cohen, A. O., Cervera, A., Tottenham, N., and Casey, B. (2018). The racially diverse affective expression (RADIATE) face stimulus set. *Psychiatry Research*, 270:1059–1067.
- Cui, X., Bray, S., and Reiss, A. L. (2010). Functional near infrared spectroscopy (NIRS) signal improvement based on negative correlation between oxygenated and deoxygenated hemoglobin dynamics. *NeuroImage*, 49(4):3039–3046.
- De Borst, A. W. and De Gelder, B. (2015). Is it the real deal? Perception of virtual characters versus humans: an affective cognitive neuroscience perspective. *Frontiers in Psychology*, 6.
- Dyck, M., Winbeck, M., Leiberg, S., Chen, Y., Gur, R. C., and Mathiak, K. (2008). Recognition Profile of Emotions in Natural and Virtual Faces. *PLOS ONE*, 3(11):e3628. Publisher: Public Library of Science.
- Ekman, P. and Friesen, W. V. (1971). Constants across cultures in the face and emotion. *Journal of personality and social psychology*, 17(2):124.
- Ekman, P. and Friesen, W. V. (1978). Facial action coding system. *Environmental Psychology & Nonverbal Behavior*.
- Faita, C., Vanni, F., Lorenzini, C., Carrozzino, M., Tanca, C., and Bergamasco, M. (2015). Perception of Basic Emotions from Facial Expressions of Dynamic Virtual

- Avatars. In De Paolis, L. T. and Mongelli, A., editors, *Augmented and Virtual Reality*, volume 9254, pages 409–419. Springer International Publishing, Cham. Series Title: Lecture Notes in Computer Science.
- Fishburn, F. A., Ludlum, R. S., Vaidya, C. J., and Medvedev, A. V. (2019). Temporal Derivative Distribution Repair (TDDR): A motion correction method for fNIRS. *NeuroImage*, 184:171–179.
- Friston, K. J. (2007). *Statistical parametric mapping: the analysis of functional brain images*. Elsevier / Academic Press, Amsterdam Boston, 1st ed edition.
- García, A. S., Fernández-Sotos, P., Vicente-Querol, M. A., Lahera, G., Rodriguez-Jimenez, R., and Fernández-Caballero, A. (2020). Design of reliable virtual human facial expressions and validation by healthy people. *Integrated Computer-Aided Engineering*, 27(3):287–299.
- Gramfort, A., Luessi, M., Larson, E., Engemann, D. A., Strohmeier, D., Brodbeck, C., Goj, R., Jas, M., Brooks, T., Parkkonen, L., and Hämäläinen, M. (2013). MEG and EEG data analysis with MNE-Python. *Frontiers in Neuroscience*, 7. Publisher: Frontiers.
- Hakim, U., De Felice, S., Pinti, P., Zhang, X., Noah, J., Ono, Y., Burgess, P. W., Hamilton, A., Hirsch, J., and Tachtsidis, I. (2023). Quantification of inter-brain coupling: A review of current methods used in haemodynamic and electrophysiological hyperscanning studies. *NeuroImage*, 280:120354.
- Hernandez, S. M. and Pollonini, L. (2020). NIRSplot: A Tool for Quality Assessment of fNIRS Scans. In *Biophotonics Congress: Biomedical Optics 2020 (Translational, Microscopy, OCT, OTS, BRAIN)*, page BM2C.5, Washington, DC. Optica Publishing Group.

- Hocke, L. M., Oni, I. K., Duszynski, C. C., Corrigan, A. V., Frederick, B. D., and Dunn, J. F. (2018). Automated Processing of fNIRS Data—A Visual Guide to the Pitfalls and Consequences. *Algorithms*, 11(5):67. Number: 5 Publisher: Multidisciplinary Digital Publishing Institute.
- Holmes, M., Aalto, D., and Cummine, J. (2024). Opening the dialogue: A preliminary exploration of hair color, hair cleanliness, light, and motion effects on fNIRS signal quality. *PLOS ONE*, 19(5):e0304356. Publisher: Public Library of Science.
- Hortensius, R., Hekele, F., and Cross, E. S. (2018). The Perception of Emotion in Artificial Agents. *IEEE Transactions on Cognitive and Developmental Systems*, 10(4):852–864.
- Hu, P., Wang, P., Zhao, R., Yang, H., and Biswal, B. B. (2023). Characterizing the spatiotemporal features of functional connectivity across the white matter and gray matter during the naturalistic condition. *Frontiers in Neuroscience*, 17. Publisher: Frontiers.
- Huppert, T. J. (2016). Commentary on the statistical properties of noise and its implication on general linear models in functional near-infrared spectroscopy. *Neurophotonics*, 3(1):010401. Publisher: SPIE.
- Kegel, L. C., Brugger, P., Frühholz, S., Grunwald, T., Hilfiker, P., Kohnen, O., Loertscher, M. L., Mersch, D., Rey, A., Sollfrank, T., Steiger, B. K., Sternagel, J., Weber, M., and Jokeit, H. (2020). Dynamic human and avatar facial expressions elicit differential brain responses. *Social Cognitive and Affective Neuroscience*, 15(3):303–317.
- Kinder, K. T., Heim, H. L. R., Parker, J., Lowery, K., McCraw, A., Eddings, R. N., Defenderfer, J., Sullivan, J., and Buss, A. T. (2022). Systematic review of fNIRS studies reveals inconsistent chromophore data reporting practices. *Neurophotonics*, 9(4):040601.

- Kocsis, L., Herman, P., and Eke, A. (2006). The modified Beer–Lambert law revisited. *Physics in Medicine & Biology*, 51(5):N91.
- Kragel, P. A. and LaBar, K. S. (2016). Decoding the Nature of Emotion in the Brain. *Trends in cognitive sciences*, 20(6):444–455.
- Kätsyri, J., Mäkäräinen, M., and Takala, T. (2017). Testing the ‘uncanny valley’ hypothesis in semirealistic computer-animated film characters: An empirical evaluation of natural film stimuli. *International Journal of Human-Computer Studies*, 97:149–161.
- Lindquist, K. A., Wager, T. D., Kober, H., Bliss-Moreau, E., and Barrett, L. F. (2012). The brain basis of emotion: A meta-analytic review. *Behavioral and Brain Sciences*, 35(3):121–143.
- Luke, R., Larson, E. D., Shader, M. J., Innes-Brown, H., Yper, L. V., Lee, A. K. C., Sowman, P. F., and McAlpine, D. (2021). Analysis methods for measuring passive auditory fNIRS responses generated by a block-design paradigm. *Neurophotonics*, 8(2):025008. Publisher: SPIE.
- Miranda de Sá, A. M. F. L., Ferreira, D. D., Dias, E. W., Mendes, E. M. A. M., and Felix, L. B. (2009). Coherence estimate between a random and a periodic signal: Bias, variance, analytical critical values, and normalizing transforms. *Journal of the Franklin Institute*, 346(9):841–853.
- Mori, M., MacDorman, K. F., and Kageki, N. (2012). The Uncanny Valley [From the Field]. *IEEE Robotics & Automation Magazine*, 19(2):98–100.
- Oliver, M. M. and Amengual Alcover, E. (2020). UIBVFED: Virtual facial expression dataset. *PLOS ONE*, 15(4):e0231266.
- Park, S., Kim, S. P., and Whang, M. (2021). Individual’s Social Perception of Virtual

- Avatars Embodied with Their Habitual Facial Expressions and Facial Appearance. *Sensors*, 21(17):5986.
- Peirce, J., Gray, J. R., Simpson, S., MacAskill, M., Höchenberger, R., Sogo, H., Kastman, E., and Lindeløv, J. K. (2019). PsychoPy2: Experiments in behavior made easy. *Behavior Research Methods*, 51(1):195–203.
- Pinti, P., Scholkmann, F., Hamilton, A., Burgess, P., and Tachtsidis, I. (2019). Current Status and Issues Regarding Pre-processing of fNIRS Neuroimaging Data: An Investigation of Diverse Signal Filtering Methods Within a General Linear Model Framework. *Frontiers in Human Neuroscience*, 12.
- Pollonini, L., Bortfeld, H., and Oghalai, J. S. (2016). PHOEBE: a method for real time mapping of optodes-scalp coupling in functional near-infrared spectroscopy. *Biomedical Optics Express*, 7(12):5104–5119. Publisher: Optica Publishing Group.
- Powell, L. J., Kosakowski, H. L., and Saxe, R. (2018). Social Origins of Cortical Face Areas. *Trends in cognitive sciences*, 22(9):752–763.
- Reddy, P., Izzetoglu, M., Shewokis, P. A., Sangobowale, M., Diaz-Arrastia, R., and Izzetoglu, K. (2021). Evaluation of fNIRS signal components elicited by cognitive and hypercapnic stimuli. *Scientific Reports*, 11(1):23457. Publisher: Nature Publishing Group.
- Sato, W., Yoshikawa, S., Kochiyama, T., and Matsumura, M. (2004). The amygdala processes the emotional significance of facial expressions: an fMRI investigation using the interaction between expression and face direction. *NeuroImage*, 22(2):1006–1013.
- Schindler, S., Zell, E., Botsch, M., and Kissler, J. (2017). Differential effects of face-realism and emotion on event-related brain potentials and their implications for the uncanny valley theory. *Scientific Reports*, 7(1):45003. Publisher: Nature Publishing Group.

- Scholkmann, F., Metz, A. J., and Wolf, M. (2014). Measuring tissue hemodynamics and oxygenation by continuous-wave functional near-infrared spectroscopy—how robust are the different calculation methods against movement artifacts? *Physiological Measurement*, 35(4):717. Publisher: IOP Publishing.
- Seabold, S. and Perktold, J. (2010). statsmodels: Econometric and statistical modeling with python. In *9th Python in Science Conference*.
- Singh, A. K. and Dan, I. (2006). Exploring the false discovery rate in multichannel NIRS. *NeuroImage*, 33(2):542–549.
- Sollfrank, T., Kohnen, O., Hilfiker, P., Kegel, L. C., Jokeit, H., Brugger, P., Loertscher, M. L., Rey, A., Mersch, D., Sternagel, J., Weber, M., and Grunwald, T. (2021). The Effects of Dynamic and Static Emotional Facial Expressions of Humans and Their Avatars on the EEG: An ERP and ERD/ERS Study. *Frontiers in Neuroscience*, 15. Publisher: Frontiers.
- Tachtsidis, I. and Scholkmann, F. (2016). False positives and false negatives in functional near-infrared spectroscopy: issues, challenges, and the way forward. *Neurophotonics*, 3(3):031405. Publisher: SPIE.
- Tak, S. and Ye, J. C. (2014). Statistical analysis of fNIRS data: A comprehensive review. *NeuroImage*, 85:72–91.
- Westgarth, M. M. P., Hogan, C. A., Neumann, D. L., and Shum, D. H. K. (2021). A systematic review of studies that used NIRS to measure neural activation during emotion processing in healthy individuals. *Social Cognitive and Affective Neuroscience*, 16(4):345–369.
- Xu, G., Zhang, M., Wang, Y., Liu, Z., Huo, C., Li, Z., and Huo, M. (2017). Functional connectivity analysis of distracted drivers based on the wavelet phase coherence of

- functional near-infrared spectroscopy signals. *PLOS ONE*, 12(11):e0188329. Publisher: Public Library of Science.
- Yücel, M. A., Selb, J. J., Huppert, T. J., Franceschini, M. A., and Boas, D. A. (2017). Functional Near Infrared Spectroscopy: Enabling routine functional brain imaging. *Current Opinion in Biomedical Engineering*, 4:78–86.

# Appendix A

## GLM Contrasts

Table A.1: Table of contrast results from the GLM analysis.

Contrast	Region	Ch Name	Coef.	Std.Err.	<i>z</i>	<i>p<sub>fdr</sub></i>
Real > Virtual	L. Occipital	S23 D15 hbt	-1.550	0.394	-3.937	0.009
Joy > Neutral	R. Parietal	S20 D29 hbt	2.611	0.623	4.194	0.001
Joy > Neutral	R. Occipital	S23 D30 hbt	-3.144	0.623	-5.050	0.000
Joy > Surprise	R. Occipital	S23 D16 hbt	-2.884	0.647	-4.460	0.001
Joy > Surprise	L. Central/Temporal	S25 D6 hbt	-2.379	0.647	-3.679	0.012
Fear > Neutral	R. Occipital	S23 D30 hbt	-2.126	0.557	-3.819	0.014
Fear > Surprise	R. Parietal	S20 D29 hbt	-2.048	0.568	-3.606	0.032
Anger > Neutral	R. Occipital	S23 D30 hbt	-3.620	0.652	-5.547	0.000
Disgust > Surprise	R. Occipital	S23 D16 hbt	-2.507	0.640	-3.920	0.005
Disgust > Surprise	L. Central/Temporal	S25 D6 hbt	-2.531	0.640	-3.958	0.005
Sadness > Neutral	L. Frontal	S4 D6 hbt	-2.257	0.601	-3.754	0.018
Sadness > Surprise	L. Frontal	S4 D6 hbt	-2.610	0.673	-3.879	0.011
Sadness > Surprise	R. Parietal	S20 D29 hbt	-2.304	0.673	-3.425	0.032

Continued on next page

Table A.1: Table of contrast results from the GLM analysis.

Contrast	Region	Ch Name	Coef.	Std.Err.	<i>z</i>	<i>p<sub>fdr</sub></i>
Neutral > Surprise	R. Parietal	S20 D29 hbt	-2.653	0.625	-4.247	0.002
Neutral > Surprise	R. Occipital	S23 D30 hbt	2.461	0.625	3.940	0.004
Real Joy > Real Disgust	R. Occipital	S23 D30 hbt	-5.344	1.093	-4.889	0.000
Real Joy > Real Sadness	R. Occipital	S24 D30 hbt	-3.816	0.964	-3.958	0.008
Real Joy > Real Neutral	R. Occipital	S23 D30 hbt	-5.786	0.980	-5.906	0.000
Real Joy > Real Surprise	R. Frontal	S9 D19 hbt	3.093	0.997	3.101	0.050
Real Joy > Real Surprise	L. Occipital	S23 D15 hbt	-3.754	0.997	-3.764	0.017
Real Joy > Real Surprise	R. Occipital	S23 D16 hbt	-3.577	0.997	-3.587	0.017
Real Joy > Real Surprise	L. Central/Temporal	S25 D6 hbt	-3.293	0.997	-3.302	0.033
Real Joy > Virtual Joy	L. Occipital	S32 D15 hbt	3.484	0.966	3.607	0.032
Real Joy > Virtual Fear	L. Occipital	S23 D15 hbt	-3.384	0.965	-3.506	0.023
Real Joy > Virtual Fear	R. Occipital	S23 D30 hbt	-3.649	0.965	-3.781	0.016
Real Joy > Virtual Disgust	L. Occipital	S23 D15 hbt	-4.428	0.986	-4.490	0.001
Real Joy > Virtual Sadness	L. Occipital	S23 D15 hbt	-4.435	0.973	-4.556	0.001
Real Joy > Virtual Surprise	R. Occipital	S23 D16 hbt	-3.197	0.949	-3.368	0.039
Real Joy > Virtual Surprise	R. Occipital	S23 D30 hbt	-3.410	0.949	-3.593	0.034
Real Fear > Real Disgust	R. Occipital	S23 D30 hbt	-4.918	1.087	-4.522	0.001
Real Fear > Real Neutral	R. Occipital	S23 D30 hbt	-5.360	0.980	-5.470	0.000
Real Fear > Virtual Joy	L. Central/Temporal	S25 D6 hbt	4.150	1.054	3.938	0.008
Real Fear > Virtual Disgust	L. Occipital	S23 D15 hbt	-4.112	1.009	-4.073	0.002
Real Fear > Virtual Disgust	L. Central/Temporal	S25 D6 hbt	4.183	1.009	4.144	0.002
Real Fear > Virtual Sadness	L. Occipital	S23 D15 hbt	-4.119	1.003	-4.109	0.004
Real Fear > Virtual Sadness	L. Central/Temporal	S25 D6 hbt	3.595	1.003	3.585	0.017

Continued on next page

Table A.1: Table of contrast results from the GLM analysis.

Contrast	Region	Ch Name	Coef.	Std.Err.	<i>z</i>	<i>p<sub>fdr</sub></i>
Real Anger > Real Disgust	R. Occipital	S23 D30 hbt	-4.697	1.117	-4.205	0.003
Real Anger > Real Neutral	R. Occipital	S23 D30 hbt	-5.139	0.983	-5.226	0.000
Real Disgust > Real Surprise	L. Frontal	S4 D6 hbt	-3.742	1.107	-3.380	0.025
Real Disgust > Real Surprise	L. Occipital	S23 D15 hbt	-4.679	1.107	-4.226	0.002
Real Disgust > Real Surprise	R. Occipital	S23 D30 hbt	4.221	1.107	3.813	0.007
Real Disgust > Virtual Fear	L. Occipital	S23 D15 hbt	-4.309	1.013	-4.252	0.002
Real Disgust > Virtual Disgust	L. Occipital	S23 D15 hbt	-5.353	1.163	-4.603	0.000
Real Disgust > Virtual Disgust	R. Occipital	S23 D30 hbt	5.028	1.163	4.323	0.001
Real Disgust > Virtual Sadness	L. Occipital	S23 D15 hbt	-5.360	1.163	-4.608	0.000
Real Disgust > Virtual Sadness	R. Occipital	S23 D30 hbt	4.254	1.163	3.657	0.013
Real Disgust > Virtual Neutral	R. Occipital	S23 D30 hbt	3.878	1.102	3.520	0.044
Real Sadness > Real Neutral	R. Occipital	S23 D30 hbt	-3.749	0.912	-4.110	0.002
Real Sadness > Real Neutral	R. Occipital	S24 D30 hbt	4.012	0.912	4.398	0.001
Real Sadness > Real Surprise	L. Frontal	S4 D6 hbt	-3.743	1.059	-3.534	0.021
Real Sadness > Real Surprise	R. Occipital	S24 D30 hbt	4.688	1.059	4.426	0.001
Real Sadness > Virtual Joy	R. Occipital	S24 D30 hbt	3.811	1.048	3.638	0.028
Real Sadness > Virtual Disgust	L. Occipital	S23 D15 hbt	-3.951	1.088	-3.633	0.029
Real Sadness > Virtual Sadness	L. Occipital	S23 D15 hbt	-3.959	1.051	-3.766	0.017
Real Neutral > Real Surprise	R. Parietal	S20 D29 hbt	-3.553	0.933	-3.809	0.007
Real Neutral > Real Surprise	R. Occipital	S23 D30 hbt	4.663	0.933	4.999	0.000
Real Neutral > Virtual Joy	R. Occipital	S23 D30 hbt	3.563	0.924	3.856	0.012
Real Neutral > Virtual Anger	L. Frontal	S4 D6 hbt	4.371	1.009	4.330	0.002
Real Neutral > Virtual Anger	R. Occipital	S23 D30 hbt	3.737	1.009	3.702	0.011

Continued on next page

Table A.1: Table of contrast results from the GLM analysis.

Contrast	Region	Ch Name	Coef.	Std.Err.	<i>z</i>	<i>p<sub>fdr</sub></i>
Real Neutral > Virtual Disgust	R. Occipital	S23 D30 hbt	5.470	1.020	5.365	0.000
Real Neutral > Virtual Sadness	L. Frontal	S4 D6 hbt	4.863	0.963	5.051	0.000
Real Neutral > Virtual Sadness	R. Occipital	S23 D30 hbt	4.696	0.963	4.877	0.000
Real Neutral > Virtual Neutral	R. Occipital	S23 D30 hbt	4.320	0.994	4.346	0.001
Real Surprise > Virtual Joy	L. Frontal	S4 D6 hbt	3.580	1.038	3.448	0.029
Real Surprise > Virtual Joy	L. Central/Temporal	S25 D6 hbt	4.185	1.038	4.030	0.006
Real Surprise > Virtual Anger	L. Frontal	S4 D6 hbt	5.443	1.096	4.966	0.000
Real Surprise > Virtual Anger	R. Frontal	S10 D17 hbt	-3.659	1.096	-3.338	0.029
Real Surprise > Virtual Anger	L. Occipital	S23 D15 hbt	3.907	1.096	3.565	0.019
Real Surprise > Virtual Disgust	L. Central/Temporal	S25 D6 hbt	4.218	1.042	4.048	0.005
Real Surprise > Virtual Sadness	L. Frontal	S4 D6 hbt	5.935	1.000	5.937	0.000
Real Surprise > Virtual Sadness	L. Central/Temporal	S7 D6 hbt	3.660	1.000	3.661	0.007
Real Surprise > Virtual Sadness	R. Parietal	S20 D29 hbt	4.101	1.000	4.102	0.002
Real Surprise > Virtual Sadness	L. Central/Temporal	S25 D6 hbt	3.630	1.000	3.631	0.007
Real Surprise > Virtual Neutral	L. Frontal	S4 D6 hbt	3.189	1.025	3.111	0.048
Real Surprise > Virtual Neutral	R. Frontal	S9 D19 hbt	-3.357	1.025	-3.275	0.048
Real Surprise > Virtual Neutral	R. Parietal	S20 D29 hbt	3.539	1.025	3.453	0.048
Real Surprise > Virtual Neutral	L. Occipital	S31 D15 hbt	-3.254	1.025	-3.174	0.048
Virtual Joy > Virtual Disgust	L. Occipital	S32 D15 hbt	-4.343	1.008	-4.308	0.002
Virtual Fear > Virtual Disgust	R. Occipital	S23 D30 hbt	3.333	0.928	3.590	0.034
Virtual Fear > Virtual Sadness	L. Frontal	S4 D6 hbt	3.597	1.021	3.522	0.044
Virtual Anger > Virtual Disgust	L. Frontal	S4 D6 hbt	-3.633	1.033	-3.518	0.019
Virtual Anger > Virtual Disgust	L. Occipital	S23 D15 hbt	-4.581	1.033	-4.436	0.001

Continued on next page

Table A.1: Table of contrast results from the GLM analysis.

Contrast	Region	Ch Name	Coef.	Std.Err.	<i>z</i>	<i>p<sub>fdr</sub></i>
Virtual Anger > Virtual Disgust	L. Central/Temporal	S25 D6 hbt	3.565	1.033	3.452	0.019
Virtual Anger > Virtual Sadness	L. Occipital	S23 D15 hbt	-4.589	1.018	-4.508	0.001
Virtual Disgust > Virtual Sadness	L. Frontal	S4 D6 hbt	4.125	1.044	3.950	0.008
Virtual Disgust > Virtual Surprise	L. Occipital	S23 D15 hbt	3.761	1.001	3.758	0.018
Virtual Sadness > Virtual Surprise	L. Occipital	S23 D15 hbt	3.768	0.978	3.853	0.012



# Appendix B

## Functional Connectivity Contrasts

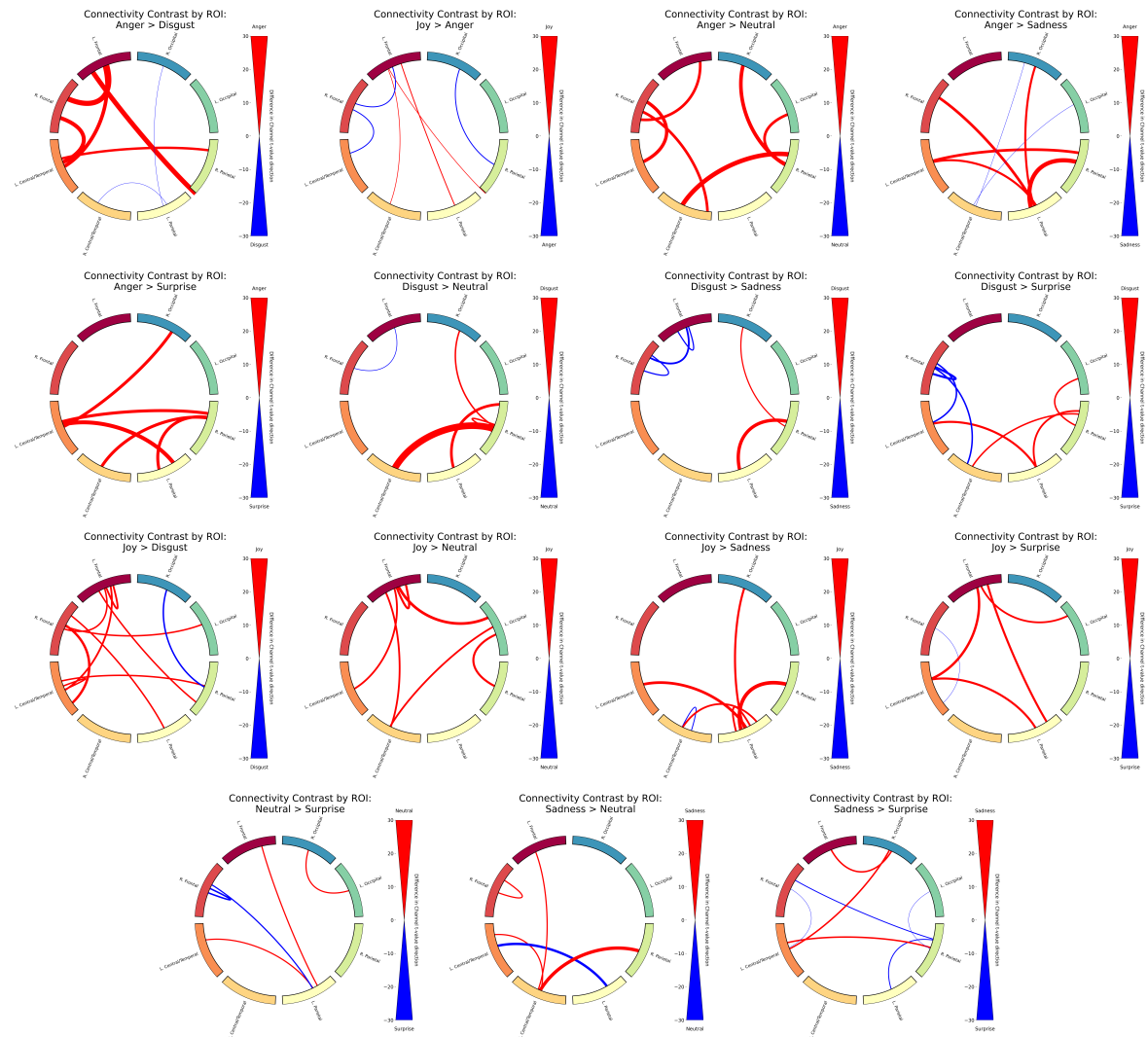


Figure B.1: Functional connectivity results for the rest of the contrasts. These are the rest of the contrasts that were not shown in 3.6.

Table B.1: Ratio of positive to negative  $t$ -values for each contrast. The ratio is calculated as  $\text{Ratio} = (\text{Number of Positive } t\text{-values} - \text{Number of Negative } t\text{-values}) / (\text{Number of Positive } t\text{-values} + \text{Number of Negative } t\text{-values})$ . For condition1 > condition2, a positive ratio indicates that condition1 has more positive  $t$ -values than condition2, while a negative ratio indicates the opposite.

Contrast	Ratio
Real > Virtual	0.632
Joy > Fear	-0.797
Joy > Anger	-0.323
Joy > Disgust	0.541
Joy > Sadness	0.622
Joy > Neutral	0.894
Joy > Surprise	0.976
Fear > Anger	0.345
Fear > Disgust	0.959
Fear > Sadness	0.865
Fear > Neutral	0.977
Fear > Surprise	0.966
Anger > Disgust	0.805
Anger > Sadness	0.709
Anger > Neutral	0.957
Anger > Surprise	0.897
Disgust > Sadness	0.099
Disgust > Neutral	0.677
Disgust > Surprise	0.172
Sadness > Neutral	0.311

Continued on next page

Table B.1: Ratio of positive to negative  $t$ -values for each contrast. The ratio is calculated as  $\text{Ratio} = (\text{Number of Positive } t\text{-values} - \text{Number of Negative } t\text{-values}) / (\text{Number of Positive } t\text{-values} + \text{Number of Negative } t\text{-values})$ . For condition1 > condition2, a positive ratio indicates that condition1 has more positive  $t$ -values than condition2, while a negative ratio indicates the opposite.

Contrast	Ratio
Sadness > Surprise	0.400
Neutral > Surprise	0.077
Real Joy > Real Fear	-0.284
Real Joy > Real Anger	-0.546
Real Joy > Real Disgust	0.881
Real Joy > Real Sadness	-0.390
Real Joy > Real Neutral	0.602
Real Joy > Real Surprise	0.306
Real Joy > Virtual Joy	0.400
Real Joy > Virtual Fear	-0.882
Real Joy > Virtual Anger	-0.985
Real Joy > Virtual Disgust	-0.636
Real Joy > Virtual Sadness	0.161
Real Joy > Virtual Neutral	0.158
Real Joy > Virtual Surprise	0.624
Real Fear > Real Anger	-0.254
Real Fear > Real Disgust	0.832
Real Fear > Real Sadness	-0.016
Real Fear > Real Neutral	0.617
Real Fear > Real Surprise	0.400

Continued on next page

Table B.1: Ratio of positive to negative  $t$ -values for each contrast. The ratio is calculated as  $\text{Ratio} = (\text{Number of Positive } t\text{-values} - \text{Number of Negative } t\text{-values}) / (\text{Number of Positive } t\text{-values} + \text{Number of Negative } t\text{-values})$ . For condition1 > condition2, a positive ratio indicates that condition1 has more positive  $t$ -values than condition2, while a negative ratio indicates the opposite.

Contrast	Ratio
Real Fear > Virtual Joy	0.395
Real Fear > Virtual Fear	-0.578
Real Fear > Virtual Anger	-0.880
Real Fear > Virtual Disgust	0.103
Real Fear > Virtual Sadness	0.525
Real Fear > Virtual Neutral	0.366
Real Fear > Virtual Surprise	0.779
Real Anger > Real Disgust	0.823
Real Anger > Real Sadness	0.115
Real Anger > Real Neutral	0.853
Real Anger > Real Surprise	0.739
Real Anger > Virtual Joy	0.858
Real Anger > Virtual Fear	-0.482
Real Anger > Virtual Anger	-0.914
Real Anger > Virtual Disgust	0.359
Real Anger > Virtual Sadness	0.507
Real Anger > Virtual Neutral	0.743
Real Anger > Virtual Surprise	0.659
Real Disgust > Real Sadness	-0.792
Real Disgust > Real Neutral	0.306

Continued on next page

Table B.1: Ratio of positive to negative  $t$ -values for each contrast. The ratio is calculated as  $\text{Ratio} = (\text{Number of Positive } t\text{-values} - \text{Number of Negative } t\text{-values}) / (\text{Number of Positive } t\text{-values} + \text{Number of Negative } t\text{-values})$ . For condition1 > condition2, a positive ratio indicates that condition1 has more positive  $t$ -values than condition2, while a negative ratio indicates the opposite.

Contrast	Ratio
Real Disgust > Real Surprise	-0.400
Real Disgust > Virtual Joy	-0.188
Real Disgust > Virtual Fear	-0.959
Real Disgust > Virtual Anger	-0.979
Real Disgust > Virtual Disgust	-0.545
Real Disgust > Virtual Sadness	-0.372
Real Disgust > Virtual Neutral	-0.373
Real Disgust > Virtual Surprise	-0.275
Real Sadness > Real Neutral	0.859
Real Sadness > Real Surprise	0.649
Real Sadness > Virtual Joy	0.694
Real Sadness > Virtual Fear	-0.333
Real Sadness > Virtual Anger	-0.825
Real Sadness > Virtual Disgust	0.036
Real Sadness > Virtual Sadness	0.308
Real Sadness > Virtual Neutral	0.489
Real Sadness > Virtual Surprise	0.885
Real Neutral > Real Surprise	-0.480
Real Neutral > Virtual Joy	-0.463
Real Neutral > Virtual Fear	-0.937

Continued on next page

Table B.1: Ratio of positive to negative  $t$ -values for each contrast. The ratio is calculated as  $\text{Ratio} = (\text{Number of Positive } t\text{-values} - \text{Number of Negative } t\text{-values}) / (\text{Number of Positive } t\text{-values} + \text{Number of Negative } t\text{-values})$ . For condition1 > condition2, a positive ratio indicates that condition1 has more positive  $t$ -values than condition2, while a negative ratio indicates the opposite.

Contrast	Ratio
Real Neutral > Virtual Anger	-0.969
Real Neutral > Virtual Disgust	-0.856
Real Neutral > Virtual Sadness	-0.550
Real Neutral > Virtual Neutral	-0.588
Real Neutral > Virtual Surprise	-0.105
Real Surprise > Virtual Joy	0.267
Real Surprise > Virtual Fear	-0.912
Real Surprise > Virtual Anger	-0.928
Real Surprise > Virtual Disgust	-0.200
Real Surprise > Virtual Sadness	0.123
Real Surprise > Virtual Neutral	0.058
Real Surprise > Virtual Surprise	0.432
Virtual Joy > Virtual Fear	-0.867
Virtual Joy > Virtual Anger	-0.979
Virtual Joy > Virtual Disgust	-0.767
Virtual Joy > Virtual Sadness	-0.203
Virtual Joy > Virtual Neutral	-0.476
Virtual Joy > Virtual Surprise	-0.150
Virtual Fear > Virtual Anger	-0.686
Virtual Fear > Virtual Disgust	0.722

Continued on next page

Table B.1: Ratio of positive to negative  $t$ -values for each contrast. The ratio is calculated as  $\text{Ratio} = (\text{Number of Positive } t\text{-values} - \text{Number of Negative } t\text{-values}) / (\text{Number of Positive } t\text{-values} + \text{Number of Negative } t\text{-values})$ . For condition1 > condition2, a positive ratio indicates that condition1 has more positive  $t$ -values than condition2, while a negative ratio indicates the opposite.

Contrast	Ratio
Virtual Fear > Virtual Sadness	0.728
Virtual Fear > Virtual Neutral	0.877
Virtual Fear > Virtual Surprise	0.908
Virtual Anger > Virtual Disgust	0.870
Virtual Anger > Virtual Sadness	0.941
Virtual Anger > Virtual Neutral	0.938
Virtual Anger > Virtual Surprise	0.990
Virtual Disgust > Virtual Sadness	0.351
Virtual Disgust > Virtual Neutral	0.436
Virtual Disgust > Virtual Surprise	0.739
Virtual Sadness > Virtual Neutral	-0.020
Virtual Sadness > Virtual Surprise	0.561
Virtual Neutral > Virtual Surprise	0.515

# Appendix C

## Memory Task

### C.1 ANOVA Results

Table C.1: Two-way ANOVA results for the effect of Face Type and Emotion and their interaction on the correct responses.

	sum_sq	df	F	PR(>F)
Intercept	261.07756	1.00000	1764.58989	0.00000
C(Face_Type)	1.17722	1.00000	7.95666	0.00481
C(Emotion)	0.73335	6.00000	0.82610	0.54946
C(Face_Type):C(Emotion)	0.40872	6.00000	0.46041	0.83797
Residual	710.47356	4802.00000		

## C.2 Memory Task No Response Distribution

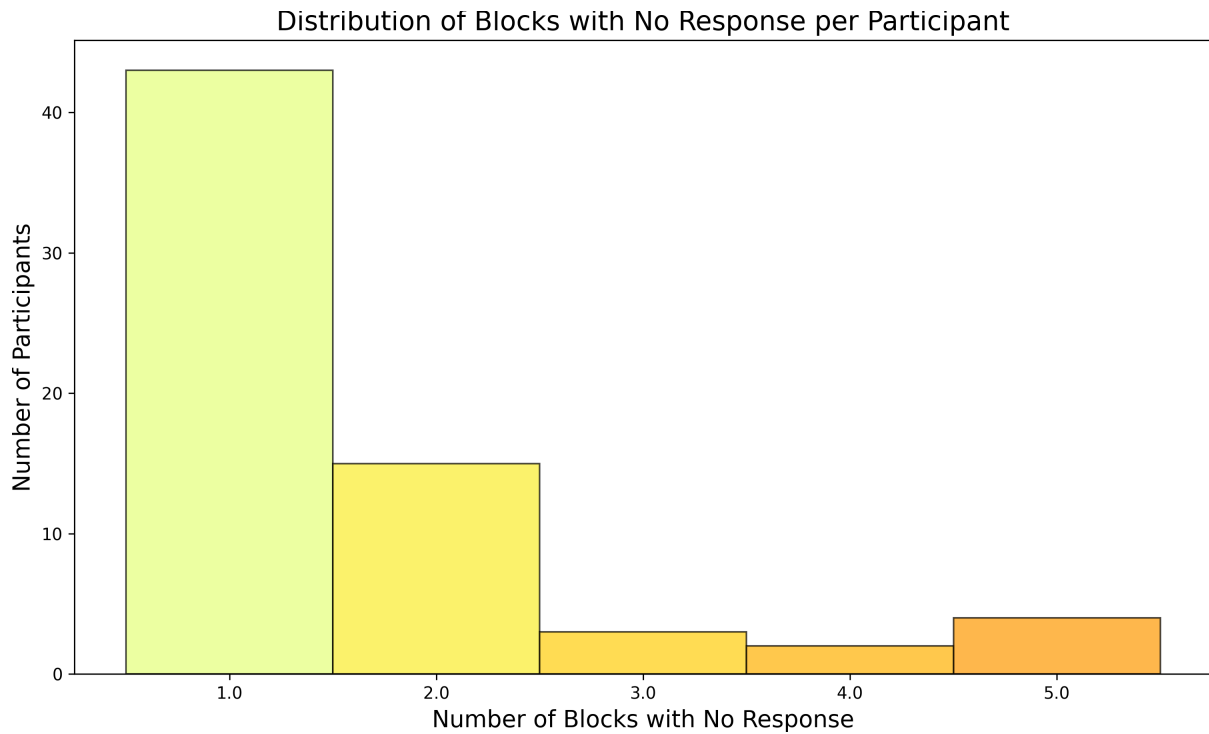


Figure C.1: Distribution of the number of no responses across the 56 blocks for each participant in the memory task.